

An Efficient, Accurate Algorithm for Calculating CO₂ 15 μm Band Cooling Rates

STEPHEN B. FELS AND M. D. SCHWARZKOPF

Geophysical Fluid Dynamics Laboratory/NOAA, Princeton University, Princeton, New Jersey 08540

A fast, accurate method for obtaining atmospheric carbon dioxide transmission functions for the 15-μm band is presented. Tables of transmissivities for CO₂ mixing ratios of 330 and 660 ppmv on standard pressure grids comprising geopotential heights ranging from 0 to 80 km and using standard temperatures are included. An algorithm for interpolating from these values to any desired temperature profile and to any other pressure grid is detailed.

1. INTRODUCTION

a. Overview

The gross thermal structure of the atmosphere between 20 and 80 km is largely determined by the balance between the heating owing to absorption of solar radiation, and infrared cooling by carbon dioxide. Any effort to model this region of the atmosphere must therefore take into account the important role played by CO₂ infrared emission. This paper sets forth in considerable detail a series of simple algorithms for calculating cooling rates owing to the 15-μm complex of CO₂ bands. The method to be described has been designed to be both computationally simple, requiring only the most modest computer resources, and, extremely accurate relative to more complex 'benchmark' computations.

The heart of this report is a description of an algorithm for calculating CO₂ transmission functions and an extensive set of tables which are crucial to the algorithm. There doubtless will be readers who are interested in understanding only enough of the method to be able to use it themselves, while there will be others who are interested in understanding why the method works and, in detail, how well. To accommodate both groups, we have included a full and detailed discussion of the algorithm, but certain technical sections may be skipped by those who are only interested in learning how the method works, rather than why (sections 1b, 1c, and 2b).

The report is divided into six major sections. In the first, we review the role played by CO₂ cooling in the atmosphere and assess the need for accurate and efficient algorithms. The second section is a detailed exposition of our scheme and explains the method by which the great bulk of the computation can be done in advance. To do this, however, requires the use of extensive tables of transmission functions whose use is described in section 3. We briefly compare our results with those of other workers in section 4. Section 5 is a summary, and section 6 contains the transmission function tables themselves.

b. The Role of CO₂ in Middle Atmospheric Dynamics, and the Need for Accurate Cooling Rates

Long-wave cooling affects the dynamics of the stratosphere and mesosphere in two related but conceptually different ways: It (1) plays a central role in determining the average thermal structure of the atmosphere, and therefore of the geostrophic wind, and (2) provides a damping mechanism for disturbances or perturbations to this steady state. It is not of

ten recognized that the accuracy required of IR calculations may be completely different, depending on which of the above two roles the cooling is called on to play. If, for example, one is interested in the propagation of internal waves through a specified mean state, the role played by IR is that of damping, and any parameterization which gives the approximately correct damping time should be adequate. On the other hand, when the mean thermal structure itself is determined in part by CO₂ cooling rates, the accuracy required is generally much higher.

We may make the latter remarks more specific by considering the middle atmosphere temperature to be determined entirely radiatively by the balance of IR cooling, which is strongly temperature dependent, and shortwave heating, which we assume is not. (We are here neglecting 'photochemical damping,' which arises from the temperature dependence of O₃ destruction reactions [Blake and Lindzen, 1973].)

Let us consider a set of vertical levels labeled by *i*, and let *T_i*, *J_i*, *Q_i* represent the equilibrium temperature, short-wave heating, and long-wave cooling at these levels. Radiative equilibrium implies that *Q_i* = *J_i*. By assumption, *Q_i* is a function of the thermal structure, that is,

$$Q_i = f_{\text{correct}}(\{T_j\}) \quad (1)$$

Suppose now that we are using a faulty IR scheme, so that when the same profile {*T_j*} is used as input, we get an incorrect set of cooling rates as output; that is, we get

$$Q'_i = f_{\text{incorrect}}(\{T_j\}) \quad (2)$$

We shall call *Q'_i* - *Q_i* = *ΔQ_i* the cooling rate error. If we now use the inaccurate algorithm to determine the incorrect equilibrium temperatures {*T'_j*}, we have

$$f_{\text{incorrect}}(\{T'_j\}) = J_i \quad (3)$$

For our purposes, it is sufficient to assume [Curtis, 1956] that

$$Q'_i = A'_i + \sum_j B'_{ij} T_j \quad (4)$$

then we have

$$A'_i + \sum_j B'_{ij} T'_j = J_i \quad (5)$$

or

$$A'_i + \sum_j B'_{ij} T_j + \sum_j B'_{ij}(T'_j - T_j) = J_i \quad (6)$$

Now

$$A'_i + \sum_j B'_{ij} T_j = Q'_i = Q_i + \Delta Q_i \quad (7)$$

so that

$$Q_i + \Delta Q_i + \sum_j B'_{ij} (T'_j - T_j) = J_i \quad (8)$$

Since by assumption, $J_i = Q_i$, we finally discover that

$$T'_i - T_i = - \sum_j (B')_{ij}^{-1} \Delta Q_i \quad (9)$$

where B'^{-1} is the inverse of B' . This formula is useful in that it allows us to use the relatively easily determined inaccuracies of a given radiative algorithm to compute the error in equilibrated temperature which will result when this algorithm is used in a model.

Some feeling for the implication of the above may be had by considering the case where the approximation scheme is local (i.e., the 'Newtonian cooling' parameterization). In this situation, B' is diagonal with $B'_{ii} = 1/\tau_i$. At 60 km, τ can be as much as 15 days [Dickinson, 1973], so that cooling rate errors of the order of 1° per day result in equilibrated temperatures which are in error by as much as 15°. Not only is this error unacceptable for many purposes, but it may also vary with position, especially latitude. When this is the case, the geostrophic winds calculated may be seriously in error, owing to the errors in calculated horizontal temperature gradients. In section 1d, we discuss briefly an algorithm for which this is true.

Taking τ to be on the order of 10 days, it is therefore reasonable to attempt to find an algorithm whose cooling rate error is not more than a few tenths of a degree per day.

c. The Need for Efficient Algorithms

Were the only role of radiative cooling the determination of a mean thermal state, it would not be necessary to calculate IR cooling very frequently in general circulation models (GCM's), especially those with no diurnal cycle. Unfortunately, the role played by CO₂ radiative transfer in damping transient motions and waves makes it necessary to calculate cooling rates far more frequently in such models. The reason for this lies in the fact that a damping mechanism which acts at regular finite time intervals Δt will only actually damp motions whose periods are greater than $2\Delta t$; those with shorter periods will be amplified rather than damped. This effect arises because of an aliasing error which occurs when a damper is applied at discrete time intervals. The wave spectrum of typical stratospheric general circulation models is sufficiently rich in waves with periods of less than 1 day to make computation of cooling rates at least several times per model day prudent. When a diurnal cycle is included in the solar radiation calculation, it may be necessary to calculate long-wave cooling rates as frequently as every few model hours.

The above requirements should make it obvious that for the purposes of upper atmosphere modeling, cooling rate algorithms must be sufficiently efficient so that each radiation computation takes only a small fraction of the time required for dynamical calculations; otherwise, the price in computational load is too great.

d. Methods Used Previously

We are aware of two basic types of methods which have been proposed for GCM CO₂ cooling calculations: those

based on the use of scaling approximations, in conjunction with table look-up of transmission functions, and those based more or less directly on the Newtonian cooling approximation.

In the first category are the methods developed by *Manabe and Strickler* [1964] and S. Manabe and R. T. Wetherald (unpublished data, 1974) for use in the Geophysical Fluid Dynamics Laboratory models, by *Sasamori* [1968] for NCAR, by *Ramanathan* [1976], and by *Ellingson and Gille* [1978]. Common to all of these methods is the calculation of cooling rates via the spectrally integrated Schwarzschild equations. Such formulations require the availability of broad-band transmission functions (cf. section 2a), and each of the above workers uses a somewhat different set of approximations for these. In every case, however, the transmissions (or emissivities) for an inhomogeneous atmospheric path are calculated by means of a scaling relation which allows use of a (hopefully) equivalent homogeneous path. The methods differ substantially in the complexity of the scaling procedure used, that of Sasamori being the simplest and those of Manabe-Wetherald, Ramanathan, and Ellingson-Gille somewhat more complex. Only the Manabe-Wetherald scheme and that of Ramanathan take into account Doppler broadening, even approximately.

The algorithm which we shall describe in section 2 is similar to the above in that it too requires spectrally integrated transmission functions. It differs radically from the others, however, in that the transmission functions used have been pre-calculated for actual inhomogeneous paths and make use of no scaling approximations. The availability of such transmission functions not only leads to a simple on-line algorithm, but it also allows their use as a benchmark against which the results of more highly parameterized methods may be measured.

A rather different approach to the computation seeks to avoid the complexities of the above methods by seeking a semiempirical relationship between the thermal structure and the cooling rates. Although this relationship is, in general, nonlinear and nonlocal, it may be always linearized about some standard temperature profile for small deviations therefrom, leading to an expression of the form (cf. (4))

$$Q_i = Q_i^0 + \sum_j B_{ij} (T_j - T_j^0) \quad (10)$$

In some situations, satisfactory accuracy is achieved by assuming B is diagonal, so that

$$Q_i \approx Q_i^0 + (T_i - T_i^0)/\tau_i \quad (11)$$

Owing to its great simplicity, this approximation (called Newtonian cooling) has enjoyed considerable use. The crucial quantities Q_i^0 and τ_i have been calculated by Dickinson [1973] in a paper which did much to popularize this approach.

Unfortunately, the accuracy of the Newtonian cooling approximation is not very high (cf. Figure 4 of Dickinson [1973] versus our Table 3d). Newtonian cooling rates are inherently independent of the spatial scale of the perturbation, a shortcoming which may be important in attempts to model the vertical structure of stratospheric waves. The linear matrix approach of (10) is capable of considerably higher accuracy, but there remains the problem of how Q_i^0 and B_{ij} are to be calculated. In practice, it is necessary to have available a more fundamental algorithm which can be used to calculate cooling rates for the standard thermal structure T_0 and for perturbations to it, so that the matrix B can be determined. The

algorithm to be set forth in the next section is well suited to this role.

2. THE NEW ALGORITHM

a. Precomputation and its Limitations

The long-wave cooling rate owing to a relatively narrow band such as the CO₂ 15-μm complex is given by

$$\frac{dT}{dt}(p) = \Delta\nu \left(\frac{g}{c_p} \right) \frac{\partial}{\partial p} \left\{ B_{\nu} [T(0)] \tau(0, p) + \int_0^{p'} \frac{\partial B_{\nu}}{\partial p'} \tau(p', p) dp' \right\} \quad (12)$$

$B_{\nu}(T)$ is the Planck function at the band center for temperature T , $\Delta\nu$ is the wave number interval, and $\tau(p, p')$ is the mean transmission function for the interval, defined as

$$\tau(p, p') = \frac{1}{\Delta\nu} \int_{\Delta\nu} dv \int_0^1 \mu d\mu \cdot \exp \left\{ -\frac{r}{\mu g} \int_p^{p'} dp'' \sum_i f_i [\nu; T(p''), p''] \right\} \quad (13)$$

In the above, μ is the cosine of the zenith angle, r is the CO₂ mass mixing ratio, g is the gravitational constant, and $f_i(\nu; T, p)$ the monochromatic intensity owing to the i th spectral line.

The accurate calculation of τ is by far the most time consuming part of the computation of cooling rates; typically, the direct evaluation of (13) (called the 'line-by-line' method) requires on the order of 10³ s to generate a 40 × 40 matrix of transmission functions, using an extremely fast computer. For most purposes, this is hopelessly slow, and makes on-line calculations of this sort impossible.

Carbon dioxide is chemically inert and has a very low freezing point, so that for the purposes of general circulation modeling its mixing ratio may be taken to be constant in space and time. This suggests that transmission functions be pre-computed off-line and be stored for use in the main calculation. To the extent that τ is independent of temperature deviations from some assumed standard profile, this is a very attractive way to proceed and has been used for tropospheric cooling rate calculations [Fels and Kaplan, 1975]. Neglect of temperature dependence is justified in the troposphere where dynamical processes, especially convection, are at least as important as radiation and where, in addition, CO₂ contributes less to long-wave cooling rates than does water vapor.

In the stratosphere and mesosphere, however, the dependence of the transmission functions $\tau(p, p')$ on the thermal structure between levels p and p' is of greater importance, primarily owing to the strong dependence of many of the weaker bands on temperature. To show this, the cooling rate for a model polar atmosphere (cf. Figure 1) has been calculated in two different ways: In the first transmission function are those computed for a polar sounding, while in the second the transmission functions used are those based on a mid-latitude sounding (Figure 1). In Figure 2 we show the difference in the cooling rates. Above 65 km there are cooling rate errors of 2°–3°/day, and rough estimates of the resultant errors in equilibrated temperatures suggest that these may be as large as 10°–15° (cf. (9)). For many purposes, therefore, use of a single set of precalculated τ 's is not sufficiently accurate, and we must seek some other method for cooling rate calculations.

It is reasonable to hope that some sort of perturbation expansion can be used to incorporate the temperature dependence of the transmission functions. To examine this possibility we may begin with a standard temperature profile $T_0(p)$

and a set of transmission functions calculated for it:

$$\begin{aligned} \tau_0(p_1, p_2) &= \frac{1}{\Delta\nu} \int_{\Delta\nu} dv \int_0^1 \mu d\mu \tau_0(p_1, p_2; \nu, \mu) \\ \tau_0(p_1, p_2; \nu, \mu) &= \exp \left\{ -\frac{r}{\mu g} \int_{p_1}^{p_2} dp' \sum_i f_i [\nu; T_0(p'), p'] \right\} \end{aligned} \quad (14)$$

If $\delta T(p')$ is a small temperature perturbation to T_0 , the resultant change in the transmission function is

$$\begin{aligned} \delta\tau(p_1, p_2) &= -\frac{1}{\Delta\nu} \left(\frac{r}{g} \right) \int_{\Delta\nu} dv \int_0^1 d\mu \tau_0(p_1, p_2; \nu, \mu) \\ &\quad \cdot \int_{p_1}^{p_2} dp' \sum_i \frac{\partial f_i}{\partial T} [\nu; T_0(p'), p'] \delta T(p') \\ &= \int_{p_1}^{p_2} dp' \delta T(p') \left\{ -\frac{r}{g} \frac{1}{\Delta\nu} \int_{\Delta\nu} dv \right. \\ &\quad \left. \cdot \int_0^1 d\mu \tau_0(p_1, p_2; \nu, \mu) \sum_i \frac{\partial f_i}{\partial T} [\nu; T_0(p'), p'] \right\} \\ &\equiv \int_{p_1}^{p_2} sp' \delta T(p') \frac{\delta\tau}{\delta T}(p_1, p_2; p') \end{aligned} \quad (15)$$

We recognize that this involves the functional derivative $\delta\tau/\delta T$, which is a function of p' , reflecting the dependence of τ on the temperature at all points p' between p_1 and p_2 . This makes the problem of precalculation difficult and time consuming. Consider, for example, a discrete version of the above linear perturbation equation:

$$\delta\tau(i, j) = \sum_{k \leq i, j} \delta T(k) \frac{\partial\tau(i, j)}{\partial T(k)} \Delta p_k \quad (16)$$

[$\partial\tau(i, j)/\partial T(k)$], the discrete analogue of the functional derivative, represents the change in $\tau(i, j)$ to a temperature perturbation at the k th level. It is therefore necessary to pre-calculate transmission functions for many different perturbed temperature profiles, an enterprise that represents a large computational burden as well as demanding a significantly larger amount of on-line storage than would be required were we only concerned with τ for a single sounding. (A method of precisely this sort has recently been described by Chou and Arking [1978].)

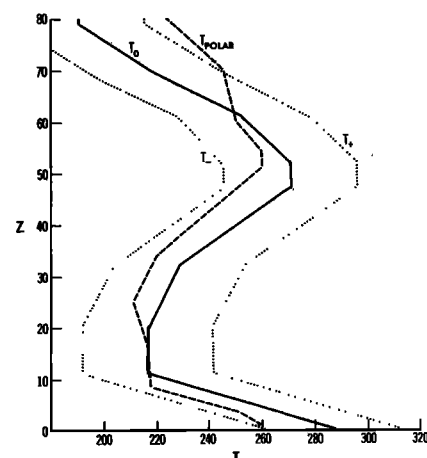


Fig. 1. Mid-latitude standard temperature profile T_0 , 'column shifted' profiles T_- and T_+ , and polar sounding.

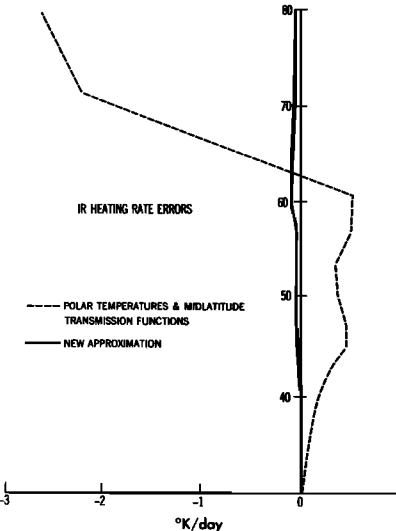


Fig. 2. Errors owing to use of mid-latitude transmission functions when calculating cooling rates for a polar sounding (dashed line) and cooling rate errors when the approximation described in this report is used to correct the mid-latitude functions for the temperature variation (solid line).

It is intuitively reasonable to expect that the detailed spatial structure of the thermal perturbation might not be of great importance. In the simplest instance of this sort, the change $\delta\tau(p_1, p_2)$ produced by an arbitrary $\delta T(p)$ might be equal to that produced by a spatially constant δT , whose magnitude Δ_{12} is just the mean value of $\delta T(p)$ on the interval (p_1, p_2) . A more complex formulation would allow Δ_{12} to be determined, using a prespecified weighting of $\delta T(p)$.

We may restate the above idea more formally by observing that the complexity of the calculation is greatly reduced if the functional derivative can be factored as

$$\frac{\delta\tau(p_1, p_2)}{\delta T(p)} = F(p_1, p_2)G(p) \quad (17)$$

In this case

$$\delta\tau(p_1, p_2) = F(p_1, p_2) \int_{p_1}^{p_2} G(p') \delta T(p') dp' \quad (18a)$$

or in discrete form

$$\delta\tau(i, j) = F(i, j) \sum_{i \leq k \leq j} G_k \delta T_k \Delta p_k \quad (18b)$$

In intuitive terms, $F_{ij} \sum_k G_k \Delta p_k$ is the change in $\tau(i, j)$ produced by a unit change in the temperature at all levels, while $\sum_k \Delta p_k G_k \delta T_k / \sum_k G_k \Delta p_k$ is the effective temperature perturbation Δ_{ij} . The determination of $F_{ij} \sum_k G_k \Delta p_k$ is very simple in practice: We consider a set of $\tau_0(i, j)$ a set of τ 's calculated for the standard temperature profile $T_0(k)$ and a set calculated for a 'column shifted' profile $T_+(k) = T_0(k) + \Delta$, which we call $\tau_+(i, j)$. Then

$$F_{ij} \sum_k G_k \Delta p_k = [\tau_+(i, j) - \tau_0(i, j)]/\Delta \quad (19)$$

The weight function G_k is not so easily determined; in practice, it was done by trial and error, guided by the considerations of the next section.

It is clear that (19), if valid, represents an enormous saving

in computation and storage. First of all, we need only pre-calculate and store a single two-dimensional matrix $F_{ij} \sum_k G_k \Delta p_k$. To do this, moreover, requires that we run the 'exact' line-by-line program only twice, once to generate $\tau_0(i, j)$ and once for $\tau_+(i, j)$. Second, for a calculation with n levels in the vertical, use of (16) requires $\sim n^3$ on-line multiplications and (19) only $\sim n^2$.

The simplifications just discussed only obtain if (19) actually holds, and in the next section we examine theoretical reasons for hoping that this is so. The real proof of the value of the method, however, is in the results that it gives, and in section 2d we shall show that our approximation method gives results of excellent accuracy.

b. Factorization of the Functional Derivative

We begin by observing that there is one situation for which factorization is trivial. If all lines are weak, we can write $\tau_r \sim 1$, so that

$$G(p') = \frac{1}{\Delta\nu} \left(\frac{r}{g} \right) \int_0^1 du \int_{\Delta\nu} dv \sum_i \frac{\partial f_i}{\partial T} [v; T_0(p'), p'] \quad (20a)$$

$$F(p_1, p_2) = 1 \quad (20b)$$

If, on the other hand, all the lines are nonoverlapping strong Lorentzian, with strengths S_b and widths γ_b , the transmission is given by

$$\begin{aligned} \tau(p_1, p_2) = \frac{1}{\Delta\nu} \left\{ 1 - \sum_i \left[\int_{p_1}^{p_2} S_b(T') \gamma_i^0 \sqrt{\frac{300}{T'}} \cdot \frac{p'}{p_0} \left(\frac{r}{g} \right) dp' \right]^{1/2} \right\} \end{aligned} \quad (21)$$

(γ_i^0 is the Lorentz width at 300° and p_0), so that

$$\begin{aligned} \delta\tau(p_1, p_2) \propto \sum_i (\gamma_i^0)^{1/2} \left\{ \int_{p_1}^{p_2} \frac{\partial}{\partial T} [S_b(T)(T)^{-1/2}] p' \delta T(p') dp' \right\} \cdot \left\{ \int_{p_1}^{p_2} S_b[T_0(p')] [T_0(p')]^{-1/2} p' dp' \right\}^{-1/2} \end{aligned} \quad (22)$$

As it stands, this clearly does not factorize. If, however, we write

$$\frac{\partial}{\partial T} [S_b(T) T^{-1/2}] = C_b h(T) \quad (23)$$

(i.e., assume that for all lines, $(\partial/\partial T)(S_b T^{-1/2})$ is proportional to a universal function of temperature), we then have

$$\begin{aligned} \delta\tau(p_1, p_2) \propto \int_{p_1}^{p_2} p' h[T_0(p')] \delta T(p') dp' \cdot \sum_i (\gamma_i^0)^{1/2} C_i \left\{ \int_{p_1}^{p_2} S_b[T_0(p')] [T_0(p')]^{-1/2} p' dp' \right\}^{-1/2} \end{aligned} \quad (24a)$$

so that

$$F(p_1, p_2) \propto \sum_i (\gamma_i^0)^{1/2} C_i \left\{ \int_{p_1}^{p_2} S_b[T_0(p')] [T_0(p')]^{-1/2} p' dp' \right\}^{-1/2} \quad (24b)$$

and

$$G(p) = p h[T_0(p)] \quad (24c)$$

There is a close connection between the above development

and the Curtis-Godson approximation in the strong limit [Rodgers and Walshaw, 1966], where

$$\tau(p_1, p_2) = 1 - c[v(p_1, p_2)]^{1/2} \quad (25a)$$

with

$$v = \int_{p_1}^{p_2} \left(\frac{r}{g} \right) p' \psi[T(p')] dp' \quad (25b)$$

Here $\psi(T)$ is a weighting function designed to incorporate approximately the effects of temperature dependent line intensity. For details as to how it is determined the reader is referred to Rodgers and Walshaw [1966].

With τ of this form, we have

$$\delta\tau(p_1, p_2) = -\frac{1}{2} c[v(p_1, p_2)]^{-1/2} \int_{p_1}^{p_2} \left(\frac{r}{g} \right) p' \frac{\partial\psi}{\partial T} \delta T(p') dp' \quad (26a)$$

and thus

$$F(p_1, p_2) = -\frac{1}{2} c[v(p_1, p_2)]^{-1/2} \left(\frac{r}{g} \right) \quad (26b)$$

and

$$G(p) = p \frac{\partial\psi}{\partial T}[T_0(p)] \quad (26c)$$

It is clear, therefore, that in the strong-line approximation, the validity of the Curtis-Godson approximation insures that the factorization property holds.

Unfortunately, for CO₂ cooling in the region between the ground and the mesopause, it is necessary to consider the simultaneous presence of both strong and weak lines. A crude idea of what is to be expected in this more complex case can be had by considering a random model, along with the Curtis-Godson approximation. It then is simple to show that

$$\tau(p_1, p_2) = f(u, v) \quad (27a)$$

where

$$u = \int_{p_1}^{p_2} \Phi[T(p')] dp' \quad (27b)$$

and

$$v = \int_{p_1}^{p_2} \psi[T(p')] p' dp' \quad (27c)$$

(The weighting function Φ is the weak-line counterpart of ψ .)

This holds not only for Lorentzian lines but for the more general Voigt profile. As before, we find that

$$\delta\tau = \frac{\partial f}{\partial u} \int_{p_1}^{p_2} \frac{\partial\Phi}{\partial T} \delta T(p') dp' + \frac{\partial f}{\partial v} \int_{p_1}^{p_2} \frac{\partial\psi}{\partial T} p' \delta T(p') dp' \quad (28)$$

The expression just derived is still not in suitable form, since it requires that we use two precomputed functions, $(\partial f / \partial u)$ and $(\partial f / \partial v)$, as well as two different weighting functions. We know, however, that for the deep atmosphere, the strong line approximation $(\partial f / \partial v) \gg (\partial f / \partial u)$ is valid, while at great heights the converse is true. We therefore are led to consider a class of ad hoc weighting functions $G(p)$, which approach $\partial\Phi / \partial T$ for very small p , and $p(\partial\psi / \partial T)$ for large p .

With G of this form, we define

$$F(p_1, p_2) = \frac{\partial f}{\partial u} \int_{p_1}^{p_2} \frac{\partial\Phi}{\partial T} dp' + \frac{\partial f}{\partial v} \int_{p_1}^{p_2} \frac{\partial\psi}{\partial T} p' dp' \quad (29)$$

then the expression

$$F(p_1, p_2) \left\{ \int_{p_1}^{p_2} G(p') \delta T(p') dp' \right\} \Big/ \left\{ \int_{p_1}^{p_2} G(p') dp' \right\} \quad (30)$$

is a good approximation to $\delta\tau(p_1, p_2)$ in any of the following circumstances: (1) p_2 is small enough so that all the lines are weak, (2) p_2 is large enough so that all the lines are strong, (3) $p_2 - p_1$ is small enough so that $G(p')$ does not vary much on this interval, or (4) $\delta T(p')$ is constant.

It is therefore not unreasonable to expect that we can find an approximation to $\delta\tau$ of the required factorized form; in section 2d we will show that this is the case, after first making one final detour to consider effects owing to the finite size of δT .

c. Second Derivative Corrections to $\delta\tau$

The entire argument in the previous section has assumed that δT is sufficiently small so that a linearized perturbation scheme is valid; this issue is completely separate from that of factorizability. It is not generally true, however, that the δT 's actually encountered will be small enough to allow linearization, as may be seen from Table 1. In this table we have considered three different sets of transmission functions: $\tau_0(i, j)$, $\tau_+(i, j)$, and $\tau_-(i, j)$. The first set is calculated by using a standard temperature profile $T(p)$, while τ_+ and τ_- are computed by using the column shifted profiles $T \pm (p) = T_0(p) \pm 25^\circ$ (cf. Figure 1). The τ 's are calculated by using the 41 pressure levels given in Table 2. Were it true that the linear perturbation method is perfectly accurate, we would have $\tau_- = 2\tau_0 - \tau_+$. Table 1 shows the fractional error committed by using this linear approximation; for many purposes it is negligible in the troposphere and lower stratosphere, being less than 1%. In the mesosphere, however, there is substantial nonlinearity, leading to errors of several percent. Since δT is often $\sim 30^\circ$ in this region, we must take account of this effect.

For perturbations which are column shifts of the form $\delta T = \text{constant}$, it is trivial to incorporate a second-order correction:

$$\begin{aligned} \tau(i, j) &= \tau_0(i, j) + [\tau_+(i, j) - \tau_-(i, j)](\delta T/50) \\ &\quad + \frac{1}{2} [\tau_+(i, j) + \tau_-(i, j) - 2\tau_0(i, j)](\delta T/25)^2 \end{aligned} \quad (31)$$

In the case where δT does vary with p , we have already shown that if factorization holds, the linear approximation gives

$$\tau(i, j) \cong \tau_0(i, j) + [\tau_+(i, j) - \tau_-(i, j)] [\Delta(i, j)/50] \quad (32)$$

with

$$\Delta(i, j) = \left(\sum_{1 \leq k \leq j} G_k \delta T_k \Delta p_k \right) \Big/ \left(\sum_{1 \leq k \leq j} G_k \Delta p_k \right) \quad (33)$$

It is therefore reasonable to hope that nonlinear effects can be included approximately by simply replacing δT in (31) by $\Delta(i, j)$, calculated by using (33).

d. The Choice of G and Verification of the Algorithm

Guided by the heuristic considerations of the previous sections, we sought an approximation of the form

$$\begin{aligned} \tau(i, j) &= \tau_0(i, j) + [\tau_+(i, j) - \tau_-(i, j)][\Delta(i, j)/50] \\ &\quad + \frac{1}{2} [\tau_+(i, j) + \tau_-(i, j) - 2\tau_0(i, j)][\Delta(i, j)/25]^2 \end{aligned} \quad (34)$$

with $\Delta(i, j)$ defined as in (33).

The only thing now at our disposal was the function $G(p)$, which we searched for empirically to give the best result for a

TABLE 1. Fractional Absorption Error in Units of Parts Per Thousand (%) Using the Approximation $\tau_- = 2\tau_0 - \tau_+$

TABLE 2. Pressure Levels Used to Calculate the Error Matrices in Tables 3a to 3h

Index (i)	Pressure, mbar
1	0.00
2	0.02
3	0.05
4	0.10
5	0.18
6	0.29
7	0.44
8	0.64
9	0.92
10	1.29
11	1.79
12	2.45
13	3.33
14	4.50
15	6.04
16	8.07
17	10.73
18	14.21
19	18.76
20	24.68
21	32.36
22	42.32
23	55.15
24	71.51
25	92.14
26	117.91
27	149.84
28	189.04
29	236.26
30	291.37
31	353.78
32	422.91
33	497.90
34	577.35
35	659.27
36	740.97
37	819.06
38	889.46
39	947.53
40	988.29
41	1013.25

variety of different cases. We expect that for large p , G should be proportional to p , while for small p , the dependence should be considerably weaker. After considerable experimentation, we found that the following expression gives excellent results:

$$G(p) = p^{0.2}[1 + (p/p_0)^{0.8}] \quad p_0 = 30 \text{ mbar} \quad (35)$$

The accuracy of this formulation remains to be demonstrated. We have done this by considering two temperature profiles which differ substantially from the mid-latitude standard $T_0(p)$. The two perturbed profiles are (1) a 200° isothermal sounding, and (2) the polar sounding mentioned previously. Tables 3a and 3b show the fractional error in the uncorrected mid-latitude absorption functions for each sounding, (i.e., $(a_{\text{true}} - a_{\text{mid-lat}})/a_{\text{true}}$). The errors are very large, over 30% in the mesosphere and troposphere for the 200° case, and 20% in the polar mesosphere, leading to unacceptable errors in the cooling rate calculations. Tables 3c and 3d show the considerable improvement which results from use of (34), with $G = 1$. The maximum error in the isothermal case has been reduced to approximately 5%, and the mesospheric error is now only 2%. Tables 3e and 3f show the fractional errors which result from use of the 'best' scaling $G(p) = p^{0.2}(1 + (p/p_0)^{0.8})$. The

dramatic improvement is evident, with errors for the isothermal case now always below 1%, and for the polar sounding generally no larger than 0.1%. These are more than adequate for any present-day modeling effort, leading (in the polar case), to heating rates which differ from the exact values by less than 0.1°/day at all heights.

In some applications it may be desirable to effect a slight saving of storage space by eliminating the 'second derivative' calculation. The errors which result for the two cases are shown in Tables 3g and 3h; in general, it seems most worthwhile to pay the modest price in storage space for the substantial increase in accuracy.

As it stands, then, the method proposed is a hybrid, in that the lion's share of the work is done off-line in precalculating the transmission matrices τ_0 , τ_+ , and τ_- ; only the final correction for effects owing to deviation of the actual profile from the assumed standard sounding are carried out on-line, along with a straightforward correction for effects owing to the finite width of the band, to be discussed next.

e. Correction for Finite Width of the 15-μm Band

The spectral interval occupied by the 15-μm complex is not really narrow enough to consider the Planck function constant, as was done in (12). If precision better than several percent is required, it is necessary to take into account the variation of B and $\partial B/\partial T$ with frequency. In principle, of course, it is only necessary to calculate transmission functions for smaller spectral intervals, say, 50 cm⁻¹, and to apply the techniques discussed above to each of these separately. This represents a large increase, both in on-line computation and in storage space and therefore is undesirable.

An alternate approach begins by observing that the quantity required for heating rate calculations is

$$\int_{\Delta\nu} B_v(T) \tau_v(p, p') d\nu = \int_{\Delta\nu} B_v(T) d\nu \int_{\Delta\nu} W_v(T) \tau_v(p, p') d\nu \quad (36a)$$

where

$$W_v(T) = B_v(T) / \int_{\Delta\nu} B_v(T) d\nu \quad (36b)$$

The 'Planck-weighted' transmission function

$$\tau(p, p'; T) = \int_{\Delta\nu} d\nu W_v(T) \tau_v(p, p') \quad (37)$$

is therefore the quantity which must actually be calculated; the problem is that it is now a function of temperature. This temperature dependence is completely separate from, and in addition to, that which arose previously from the line intensity effect and cannot be handled in the same fashion. The line intensity effect depends on the temperature along the entire path between p and p' , while the effect under consideration involves only the temperature at p' .

Unfortunately, this temperature dependence of $\tau(p, p'; T)$ is not negligible, as Table 4 shows. We show there the quantity $\tau(0, p; T)$ for $p = 0.25$ mbar, $p = 90.0$ mbar, and $p = 1013.25$ mbar for several temperatures ranging from 190° to 310°. The temperature dependence is several percent, so that as stated previously, it cannot be ignored. Fortunately, however, most of this dependence can be very simply allowed for, since it turns out that to a good approximation

TABLE 3a. Fractional Absorption Error (%) in Mid-Latitude Transmission Functions Compared With Exact Functions for a 200° Sounding

TABLE 3b. Same as Table 3a, but Mid-Latitude Functions Compared With Exact Functions for a Polar Sounding

TABLE 3c. Fractional Absorption Error (%) When Mid-Latitude Functions are Corrected to a 200° Sounding Using a Weighting Function $G = 1$

TABLE 3d. Same as Table 3c, but for the Polar Case

TABLE 3e. Fractional Absorption Error (%) When Mid-Latitude Functions are Corrected to a 200° Sounding Using the Scaling $G(p) = p^{0.2} (1 + (p/p_0)^{0.8})$

TABLE 3f. Same as Table 3e, but for the Polar Case

TABLE 3g. Fractional Absorption Error (%) When the 'Second Derivative' Term is Dropped From the Correction to a 20° Sounding

TABLE 3*n*. Same as Table 3*g*, but for the Polar Case

TABLE 4. Values of the 'Planck-Weighted' Absorption From $p = 0$ to $p = 0.25, 90$, and 1013.25 mbar, as a Function of Temperature

p	190°	220°	250°	280°	310°
0.25 mbar	0.003013 (0.003017)	0.003060 (0.003055)	0.003079 ...	0.003083 (0.003088)	0.003080 (0.003085)
	0.1957 (0.1957)	0.1986 (0.1982)	0.1997 ...	0.1999 (0.2003)	0.1997 (0.2001)
90 mbar	0.4923 (0.4930)	0.4996 (0.4992)	0.5031 ...	0.5047 (0.5046)	0.5054 (0.5041)

The figures in parentheses are the corresponding values calculated by using the method of section 2e.

$$[1.000 - \tau(p, p'; T)]/[1.000 - \tau(p, p'; 250)] = f(T) \quad (38a)$$

$$f(T) = 1 + 1.833 \times 10^{-4}(T - 250)[1 - 0.01364(T - 250)] \quad (38b)$$

Thus the blackbody effect can be incorporated in our formalism by using a single set of $\tau(p, p')$ calculated by using the formula

$$\tau(p, p'; 250) = \int_{\Delta\nu} \tau_{\nu}(p, p') B_{\nu}(250) d\nu / \int_{\Delta\nu} B_{\nu}(250) d\nu \quad (39)$$

The final on-line correction is actually extremely simple to make, involving only the formula

$$\tau(p, p'; T) = 1.000 - [1.000 - \tau(p, p'; 250)]f(T) \quad (40)$$

In fact, the situation is even simpler than this, since we are usually concerned with the computation of cooling rates, which involves the derivative of τ with respect to p . From (40) we have

$$\frac{\partial\tau}{\partial p}(p, p'; T) = \frac{\partial\tau}{\partial p}(p, p'; 250)f(T) \quad (41)$$

This shows that rather than correcting the transmission functions, in practice it is only necessary to correct the source function $\int_{\Delta\nu} B_{\nu}(T) d\nu$ by multiplying it by $f(T)$.

f. Summary of the Algorithm

Assuming that one has at hand a set of precalculated matrices $\tau_0(i, j)$, $\tau_+(i, j)$, and $\tau_-(i, j)$ appropriate to the vertical level structure used the on-line calculations are simple:

1. Calculate $\Delta(i, j)$ by using (33), with G determined by (35).
2. Calculate τ_y by using (34).
3. Correct for the blackbody effect by using (38b) and (40).
4. Compute the cooling rates by using (12).

Of course, there remains the important practical matter of how τ_0 , τ_+ , and τ_- are to be calculated off-line, and this is the subject of section 3. Before taking this up, however, it is appropriate to outline the relationship between our algorithm and the Curtis matrix approach used in section 1.

The cooling rate Q_i at level i may be written schematically as

$$\begin{aligned} Q_i &= \sum_j \tau_{ij} B_j \\ &= Q_i^0 + \sum_j [\tau_y^0(B_j - B_j^0) + (\tau_y - \tau_y^0)B_j^0] \\ &\quad + \sum_j (\tau_y - \tau_y^0)(B_j - B_j^0) \end{aligned} \quad (42)$$

Here τ_{ij} and B_j are the transmission functions and blackbody functions for the actual temperature profile, respectively, τ_y^0 and B_j^0 , those for the standard profile; and Q_i^0 , the cooling rate for the standard profile.

The method we have described retains all of these terms but introduces a computationally simple approximation for $\tau_y - \tau_y^0$ which involves terms both linear and quadratic in $T_k - T_k^0$. The Curtis matrix formulation, on the other hand, is a linearization, and therefore effectively drops the last term in (41) at the same time linearizing both $B_j - B_j^0$ and $\tau_{ij} - \tau_{ij}^0$ in the variables $T_k - T_k^0$:

$$Q_i \approx Q_i^0 + \sum_j \left\{ \tau_y \frac{\partial B}{\partial T_j} + \sum_k \frac{\partial \tau_{ik}^0}{\partial T_j} B_k^0 \right\} (T_k - T_k^0) \quad (43)$$

The linearization in $T_k - T_k^0$ is not really central to the Curtis method, for one could equally well work directly with the blackbody functions rather than the temperature. The dropping of the last term in (41) is, however, crucial and can introduce substantial errors; for temperature differences of the order of 50°, $(B_j - B_j^0)/B_j$ is of the order of 1.

3. DESCRIPTION OF THE TRANSMISSION FUNCTION TABLES

a. The Need for Tables of Transmission Functions

The most important practical requirement for use of the algorithm explained in the previous section is a method for precalculation of the transmission function matrices $\tau_0(p_i, p_j)$, $\tau_+(p_i, p_j)$, and $\tau_-(p_i, p_j)$ for whatever vertical level scheme is used. Unless the user is blessed with large amounts of computer time and the rather sophisticated programs required for a line-by-line computation, direct calculation of the τ 's is impossible. To circumvent this problem, we have precalculated sets of τ matrices on a grid whose high vertical resolution makes it possible to interpolate them to any other set of vertical levels desired. It is these tables which constitute the core of this report.

b. Organization of the Tables

As was discussed previously, the perturbation algorithm requires that we have available three τ matrices, one for the standard profile (τ_0) and two for the perturbed profiles (τ_+ and τ_-). Since the use and organization of the tables is in all respects the same for each of the three sets, we will describe only the τ_0 tables.

Transmission function matrices are given for two different level structures, one useful for the atmosphere above 10 mbar and one for that below, although there is a certain amount of overlap. The reference pressures are given in Table 5, along with standard temperatures and geopotential heights. There

are 49 pressures in the upper set and 57 in the lower. Since for some purposes it is desirable to have the levels at approximately equal increments of height, while for others equal spacing in pressure is more useful, the structure chosen represents a crude compromise. Values are to be found in Table 6.

Details of the line-by-line calculation are discussed in the next section; it is only necessary here to mention that functions are first calculated for the seven 50-cm⁻¹-wide bands from 500 to 850 cm⁻¹, and then consolidated, using the formula

$$\tau(p_i, p_j) = \sum_{n=1}^7 \tau_n(p_i, p_j) B_n(250) / \sum_{n=1}^7 B_n(250) \quad (44)$$

As was explained in section 2e, a simple correction to these τ 's allows for shifts in the position of the blackbody function.

There are circumstances in which it may be useful to have available the individual 50-cm⁻¹ matrices. These are too voluminous to publish here, but are available on microfiche.

Since one active area of research is the examination of the effects of increased CO₂ levels in the earth's atmosphere, we have thought it desirable to include a set of tables appropriate to an atmosphere whose CO₂ mixing ratio is approximately twice the 1978 value (i.e., 660 ppmv). These tables are given for the same level structure as the standard set, the only difference being that the unperturbed thermal structure is somewhat different, having been modified in accordance with the results of model calculations on the probable effect of increased atmospheric CO₂ amounts [Fels et al., 1980].

c. Interpolation to Arbitrary Pressures

Use of the tables requires that one be able to interpolate accurately to find $\tau(p, p')$ for arbitrary p and p' . After considerable experimentation, we have discovered that the nonlinear scheme to be described works extremely well.

We shall assume for the sake of illustration that $p < p'$, and $p' \leq 10$ mbar. If this is true, we are only concerned with the 'upper atmosphere' table. If, on the other hand, $10 \text{ mbar} > p'$, we use the 'lower atmosphere' table (regardless of p) which actually has 15 levels above 10 mbar.

The recommended procedure is designed to interpolate accurately in the region where τ varies especially rapidly as a function of p and p' , and linear schemes fail. It exploits several observations about the dependence of τ on p and p' :

1. In the region $|p - p'|/p \ll 1$, the absorption is close to that for a homogeneous path, and it is precisely in this region that nonlinearity is most important.

2. For homogeneous paths the dependence on the absorber amount u is approximately as $u^{1/2}$ for small u , and as $\log u$ for large u [Howard et al., 1956].

3. In the homogeneous path case, $|p - p'|$ is proportional to u .

The above remarks suggest that we introduce a new variable $y = \log(\beta + |p - p'|^{1/2})$, which behaves as $|p - p'|^{1/2}$ for $|p - p'|^{1/2} \ll \beta$, and as $\log|p - p'|$ for $|p - p'|^{1/2} \gg \beta$. By trial and error we find that $\beta = 2$ mbar makes τ quite linear in y for $|p - p'| \ll p$. We, therefore, consider τ as a function of $x = p$, and y , with $\tau(p - p') = f(x, y)$, and seek a simple interpolation formula for f . We begin by finding i and j such that $p_i \leq p \leq p_{i+1}$, $p_j \leq p' \leq p_{j+1}$, and by entering the tables to find the four quantities

$$f_{ij} = \tau(p_i, p_j)$$

$$f_{i+1,j+1} = \tau(p_{i+1}, p_{j+1})$$

$$f_{ij+1} = \tau(p_i, p_{j+1})$$

$$f_{i+1,j+1} = \tau(p_{i+1}, p_{j+1})$$

The function $f(x, y)$ has a Taylor series about the point $x_0 = p_i$, $y_0 = \log(\beta + |p_i - p_j|^{1/2})$ of the form

$$f(x, y) = f(x_0, y_0) + \left(\frac{\partial f}{\partial x} \right) (x - x_0) + \left(\frac{\partial f}{\partial y} \right) (y - y_0) + \left(\frac{\partial^2 f}{\partial x \partial y} \right) (x - x_0)(y - y_0) \dots \quad (45)$$

By truncating the series with the above three terms, it is possible to calculate the partial derivatives in terms of the four

TABLE 5. Pressures, Temperatures, and Approximate Geopotential Heights for Grids on Which the Transmission Functions of Table 6 and Tables 6-1 Through 6-12 (on Microfiche) are Computed

Index (i)	Pressure, mbar	Temperature	Temperature	Geo- potential, km
		for 1 × CO ₂	for 2 × CO ₂	
<i>Upper Atmosphere Grid</i>				
1	0.000	190.54	186.92	∞
2	0.005	190.62	187.00	83.3
3	0.010	193.00	188.88	79.4
4	0.015	198.78	193.81	77.1
5	0.020	203.23	197.41	75.5
6	0.025	206.83	200.15	74.1
7	0.030	209.88	202.63	73.0
8	0.035	212.55	205.27	72.1
9	0.040	214.93	207.62	71.3
10	0.045	217.02	209.69	70.6
11	0.050	218.92	211.55	69.9
12	0.060	223.90	216.49	68.7
13	0.070	227.68	220.21	67.7
14	0.080	231.02	223.48	66.8
15	0.090	234.06	226.45	66.0
16	0.100	238.12	230.39	65.2
17	0.120	242.82	234.95	64.0
18	0.140	246.92	238.82	63.0
19	0.160	250.56	242.21	62.0
20	0.180	253.25	244.65	61.1
21	0.200	255.77	246.77	60.3
22	0.250	258.81	249.54	58.6
23	0.300	261.34	251.79	57.3
24	0.350	263.53	253.76	56.1
25	0.400	265.47	255.92	55.0
26	0.450	267.21	257.08	54.1
27	0.500	269.51	259.15	53.3
28	0.600	270.65	260.13	51.8
29	0.700	270.65	259.98	50.6
30	0.800	270.65	259.84	49.6
31	0.900	270.65	259.70	48.6
32	1.000	270.65	259.52	47.7
33	1.200	267.18	256.03	46.3
34	1.400	264.07	252.91	45.1
35	1.600	261.38	250.25	44.1
36	1.800	258.99	247.90	43.2
37	2.000	255.45	244.57	42.4
38	2.500	251.25	240.84	40.8
39	3.000	247.85	237.85	39.4
40	3.500	244.97	235.37	38.2
41	4.000	242.45	233.13	37.3
42	4.500	240.26	231.18	36.5
43	5.000	237.38	228.64	35.8
44	6.000	234.14	225.81	34.5
45	7.000	231.41	223.25	33.5
46	8.000	229.07	220.94	32.6
47	9.000	228.05	220.01	31.8
48	10.000	216.65	214.06	31.1
49	100.000			16.2

TABLE 5. (continued)

Index (i)	Pressure, mbar	Temperature for 1 × CO ₂	Temperature for 2 × CO ₂	Geo- potential, km
<i>Lower Atmosphere Grid</i>				
1	0.00	241.71	233.88	∞
2	0.25	263.53	253.76	58.6
3	0.50	270.65	259.98	53.3
4	1.00	268.02	256.87	47.7
5	1.50	260.76	249.65	44.6
6	2.00	255.45	244.57	42.4
7	2.50	251.25	240.84	40.8
8	3.00	246.37	236.57	39.4
9	4.00	241.35	232.15	37.3
10	5.00	237.38	228.64	35.8
11	6.00	234.14	225.81	34.5
12	7.00	231.41	223.25	33.5
13	8.00	229.07	220.94	32.6
14	9.00	228.05	220.01	31.8
15	10.00	227.07	219.45	31.1
16	12.00	225.97	218.84	29.9
17	14.00	225.02	218.29	28.9
18	16.00	224.20	217.86	28.0
19	18.00	223.47	217.50	27.2
20	20.00	222.74	217.19	26.5
21	22.50	222.02	217.09	25.7
22	25.00	221.06	217.08	25.0
23	30.00	219.99	216.46	23.8
24	35.00	219.07	215.87	22.8
25	40.00	218.27	215.24	22.0
26	45.00	217.56	214.71	21.3
27	50.00	216.65	214.06	20.5
28	60.00	216.65	214.36	19.5
29	70.00	216.65	214.52	18.5
30	80.00	216.65	214.62	17.6
31	90.00	216.65	214.65	16.8
32	100.00	216.65	215.12	16.2
33	120.00	216.65	216.50	15.0
34	140.00	216.65	216.65	14.0
35	160.00	216.65	216.65	13.2
36	180.00	216.65	216.65	12.5
37	200.00	216.65	216.65	11.7
38	225.00	218.65	218.65	11.0
39	250.00	224.84	224.84	10.4
40	300.00	232.09	232.09	9.2
41	350.00	238.49	238.49	8.1
42	400.00	244.25	244.25	7.2
43	450.00	249.47	249.47	6.3
44	500.00	254.27	254.27	5.6
45	550.00	258.70	258.70	4.8
46	600.00	262.84	262.84	4.2
47	650.00	266.72	266.72	3.6
48	700.00	270.37	270.37	3.0
49	750.00	273.82	273.82	2.5
50	800.00	277.10	277.10	1.9
51	850.00	280.22	280.22	1.5
52	900.00	283.20	283.20	1.0
53	950.00	286.05	286.05	0.5
54	1000.00	287.79	287.79	0.1
55	1013.25	289.14	289.14	0.0
56	1050.00	291.41	291.41	-0.3
57	1100.00	292.72	292.72	-0.7

The temperatures are assumed to be isothermal between the pressure levels.

tabulated values of f :

$$f_y = (f_{i+1,j} - f_{i,j}) / (y_{i+1,j} - y_{i,j}) \quad (46a)$$

$$f_{xy} = [f_{i+1,j+1} - f_{i+1,j} - f_y(y_{i+1,j+1} - y_{i+1,j})] / [(x_{i+1} - x_i) \\ \cdot (y_{i+1,j+1} - y_{i+1,j})] \quad (46b)$$

$$f_x = [f_{i+1,j} - f_{i,j} - [f_y + f_{xy}(x_{i+1} - x_i)] \\ \cdot (y_{i+1,j} - y_{i,j})] / (x_{i+1} - x_i) \quad (46c)$$

here $x_i = p_i$, $y_{i,j} = \log(\beta + |p_i - p_j|^{1/2})$, etc.
The final interpolation formula is, therefore,

$$f(x, y) = f_y + f_x(x - x_i) + f_y(y - y_i) \\ + f_{xy}(x - x_i)(y - y_i) \quad (47)$$

where x and y are defined as $x = p$, $y = \log(\beta + |p - p'|^{1/2})$.

The interpolation scheme described has been tested by comparing values of τ calculated from the line-by-line program for a 41-level grid with the values obtained by interpolation; the fractional absorption errors never exceed one part in a thousand. A Fortran program for interpolating to any desired set of pressures is available from the authors on the same tape which contains the precomputed transmission functions.

d. Details of the Line-by-Line Program

The tables in the report were calculated by use of a sophisticated program which is a substantially modified version of a code provided by R. Drayson [see Drayson, 1967]. The program is a numerical evaluation of (14); some relevant characteristics are discussed below.

1. The individual lines taken into account number over 3800. These come from the 19 bands listed in Table 7, along with their band centers and band intensities. The line positions, widths, and intensities have been taken from the 1978 version of the AFGL catalogue of line parameters [Rothman and Benedict, 1978]. It is important to note that whereas the individual line intensities obtained from the AFGL tape include the effect of stimulated emission, the band intensities quoted in McClatchey et al. [1973] and Rothman and Benedict [1978] do not. These band intensities must therefore be multiplied by the factor $[1 - \exp(-1.439 \Delta E/T)]$, where ΔE is the difference (in cm^{-1}) in the energy at the upper and lower state of the transition of a band and $T = 296^\circ\text{K}$.

There are some experimental uncertainties in the strengths of various lesser bands and in the line widths; these uncertainties and their effect on the calculations will be discussed in section 4. Lines whose intensities are less than $10^{-6} \text{ cm}^{-1} (\text{cm-atm})_{300\text{K}}^{-1}$ have not been included. A method for approximating the error owing to these neglected lines is under development.

2. The line profile used takes into account both Voigt effects (near line centers), and the sub-Lorentzian profiles of CO₂ lines (in the far wings). The Voigt profile is used between 0 and 100 mbar and is calculated with the algorithm of Hui et al. [1977]. Below this height, Voigt effects are negligible. The line width is assumed to vary linearly with pressure (in the Lorentz region) and as the inverse square root of temperature.

Sub-Lorentzian behavior of the wings of lines has been studied extensively in the 4.3-μm CO₂ band [Burch et al., 1969; Winters et al., 1964; Susskind and Mo, 1978]. There has been less work done on the 15-μm complex, but there is no question that, here, too, the wings are strongly sub-Lorentzian. In the absence of more detailed models, we have adopted the simple device of assuming that all absorption ceases a distance r_c from the line center. (This naturally requires that the profile be renormalized.)

By comparison of our computed results with the laboratory spectra of Gryvnak et al. [1976] and Gryvnak and Burch [1978],

TABLE 6. Transmission Function Table $\tau_0(I, J)$, Lower Atmosphere, 330 ppmb

	1	2	3	4	5	6	7	8	9	10
1	1.000000	0.996921	0.995130	0.992038	0.989328	0.986876	0.984580	0.982395	0.978259	0.974347
2	0.996921	1.000000	0.996002	0.992463	0.989617	0.987099	0.984763	0.982552	0.978383	0.974452
3	0.995130	0.996002	1.000000	0.993420	0.990238	0.987572	0.985151	0.982883	0.978645	0.974672
4	0.992038	0.992463	0.993420	1.000000	0.992559	0.989206	0.986442	0.983965	0.979478	0.975363
5	0.989328	0.989617	0.990238	0.992559	1.000000	0.992002	0.988441	0.985559	0.980646	0.976302
6	0.986876	0.987099	0.987572	0.989206	0.992002	1.000000	0.991499	0.987755	0.982126	0.977450
7	0.984580	0.984763	0.985151	0.986442	0.988441	0.991499	1.000000	0.991043	0.984027	0.978852
8	0.982395	0.982552	0.982883	0.983965	0.985559	0.987755	0.991043	1.000000	0.986548	0.980571
9	0.978259	0.978383	0.978645	0.979478	0.980646	0.982126	0.984027	0.986548	1.000000	0.985511
10	0.974347	0.974452	0.974672	0.975363	0.976302	0.977450	0.978852	0.980571	0.985511	1.000000
11	0.970598	0.970690	0.970882	0.971479	0.972276	0.973227	0.974359	0.975701	0.979222	0.984607
12	0.966975	0.967057	0.967230	0.967761	0.968458	0.969278	0.970236	0.971352	0.974161	0.978027
13	0.963458	0.963533	0.963690	0.964171	0.964795	0.965519	0.966356	0.967318	0.969683	0.972782
14	0.960031	0.960101	0.960247	0.960688	0.961256	0.961908	0.962653	0.963502	0.965556	0.968173
15	0.956668	0.956733	0.956869	0.957279	0.957801	0.958393	0.959067	0.959828	0.961649	0.963924
16	0.950109	0.950167	0.950288	0.950648	0.951100	0.951605	0.952171	0.952804	0.954291	0.956104
17	0.943769	0.943822	0.943931	0.944255	0.944655	0.945097	0.945586	0.946129	0.947386	0.948897
18	0.937641	0.937690	0.937791	0.938086	0.938446	0.938839	0.939272	0.939746	0.940837	0.942131
19	0.931715	0.931760	0.931853	0.932127	0.932455	0.932810	0.933197	0.933620	0.934582	0.935713
20	0.925981	0.926023	0.926111	0.926365	0.926668	0.926993	0.927344	0.927724	0.928585	0.929588
21	0.919070	0.919110	0.919192	0.919427	0.919703	0.919997	0.920311	0.920650	0.921410	0.922288
22	0.912431	0.912468	0.912545	0.912763	0.913019	0.913287	0.913572	0.913878	0.914558	0.915338
23	0.899898	0.899932	0.900001	0.900195	0.900419	0.900648	0.900889	0.901145	0.901706	0.902340
24	0.888274	0.888304	0.888368	0.888543	0.888743	0.888945	0.889154	0.889373	0.889851	0.890383
25	0.877463	0.877491	0.877549	0.877711	0.877892	0.878073	0.878258	0.878451	0.878866	0.879324
26	0.867387	0.867413	0.867468	0.867617	0.867784	0.867948	0.868115	0.868286	0.868654	0.869054
27	0.857979	0.858003	0.858055	0.858195	0.858349	0.858500	0.858652	0.858807	0.859135	0.859491
28	0.840935	0.840956	0.841003	0.841128	0.841264	0.841395	0.841524	0.841654	0.841926	0.842216
29	0.825820	0.825841	0.825883	0.825997	0.826119	0.826235	0.826347	0.826460	0.826692	0.826935
30	0.812364	0.812384	0.812423	0.812528	0.812640	0.812743	0.812844	0.812944	0.813146	0.813354
31	0.800337	0.800354	0.800391	0.800489	0.800592	0.800686	0.800777	0.800867	0.801046	0.801229
32	0.789533	0.789550	0.789584	0.789676	0.789772	0.789860	0.789943	0.790024	0.790186	0.790348
33	0.770917	0.770933	0.770964	0.771046	0.771131	0.771208	0.771280	0.771349	0.771484	0.771619
34	0.755425	0.755439	0.755468	0.755543	0.755620	0.755689	0.755753	0.755814	0.755931	0.756046
35	0.742246	0.742259	0.742286	0.742356	0.742427	0.742489	0.742548	0.742602	0.742707	0.742808
36	0.730795	0.730807	0.730832	0.730898	0.730964	0.731022	0.731076	0.731126	0.731221	0.731312
37	0.720653	0.720665	0.720689	0.720751	0.720813	0.720868	0.720917	0.720964	0.721051	0.721134
38	0.709373	0.709384	0.709406	0.709464	0.709523	0.709573	0.709619	0.709662	0.709742	0.709817
39	0.698927	0.698937	0.698959	0.699013	0.699068	0.699115	0.699158	0.699198	0.699272	0.699340
40	0.678893	0.678902	0.678921	0.678970	0.679018	0.679059	0.679097	0.679131	0.679194	0.679252
41	0.659936	0.659945	0.659961	0.660005	0.660048	0.660084	0.660116	0.660146	0.660201	0.660251
42	0.642150	0.642157	0.642172	0.642211	0.642249	0.642281	0.642309	0.642335	0.642383	0.642426
43	0.625548	0.625554	0.625568	0.625602	0.625636	0.625664	0.625689	0.625712	0.625754	0.625791
44	0.610092	0.610098	0.610110	0.610141	0.610171	0.610196	0.610218	0.610238	0.610274	0.610307
45	0.595653	0.595658	0.595669	0.595697	0.595723	0.595746	0.595766	0.595784	0.595816	0.595845
46	0.582151	0.582156	0.582166	0.582190	0.582215	0.582235	0.582252	0.582268	0.582297	0.582322
47	0.569515	0.569519	0.569528	0.569551	0.569572	0.569590	0.569606	0.569621	0.569646	0.569668
48	0.557678	0.557682	0.557690	0.557710	0.557730	0.557746	0.557761	0.557774	0.557796	0.557816
49	0.546582	0.546586	0.546593	0.546612	0.546629	0.546644	0.546657	0.546669	0.546689	0.546707
50	0.536173	0.536176	0.536183	0.536200	0.536216	0.536229	0.536241	0.536251	0.536270	0.536286
51	0.526384	0.526386	0.526393	0.526408	0.526423	0.526446	0.526455	0.526472	0.526487	
52	0.517158	0.517161	0.517166	0.517180	0.517194	0.517205	0.517215	0.517223	0.517239	0.517252
53	0.508451	0.508453	0.508459	0.508472	0.508484	0.508494	0.508503	0.508511	0.508525	0.508537
54	0.500222	0.500224	0.500229	0.500241	0.500252	0.500262	0.500270	0.500277	0.500290	0.500301
55	0.498116	0.498118	0.498123	0.498134	0.498146	0.498155	0.498163	0.498170	0.498182	0.498193
56	0.492429	0.492431	0.492436	0.492447	0.492458	0.492466	0.492474	0.492481	0.492492	0.492502
57	0.485036	0.485038	0.485042	0.485052	0.485062	0.485070	0.485077	0.485083	0.485094	0.485103

we have determined that $\nu_c = 3 \text{ cm}^{-1}$ gives excellent agreement with experiment, while $\nu_c = 1 \text{ cm}^{-1}$ gives too little absorption, and $\nu_c = 10 \text{ cm}^{-1}$ too much. Details of this study will be published elsewhere. We have therefore used the cutoff $\nu_c = 3 \text{ cm}^{-1}$ in our tables.

3. The angular integration is performed by means of a four-point Gaussian quadrature on the interval $0 \leq \mu \leq 1$.

4. The variation of g with height is accounted for.

4. COMPARISON OF RESULTS

The accuracy of the CO₂ transmission function algorithm presented in section 3 may be considered in two ways. In the first of these, the calculation of transmission functions for a standard temperature profile, performed by the line-by-line program, may be compared with transmission functions for the same profile computed by other investigators. In the second,

transmission functions computed by the new algorithm for nonstandard temperature profiles may be compared to those computed by the line-by-line program for the same profiles. This comparison has already been discussed in section 3 and shown in Tables 3a-3h. Therefore, this section will compare the line-by-line program results with other results. The comparison may be divided into two categories: (1) differences in results owing to uncertainties in CO₂ line parameters (band strengths, centers and line widths) and (2) differences owing to the treatment of CO₂ line profiles and owing to temperature effects on these lines.

a. Comparison of CO₂ Line Parameters

As we have indicated in section 3d, the line-by-line program we have employed uses line centers, intensities, and widths given in the revised AFGL catalog described in Roth-

TABLE 6. (continued)

	11	12	13	14	15	16	17	18	19	20
1	0.970598	0.966975	0.963458	0.960031	0.956668	0.950109	0.943769	0.937641	0.931715	0.925981
2	0.970690	0.967057	0.963533	0.960101	0.956733	0.950167	0.943822	0.937690	0.931760	0.926023
3	0.970882	0.967230	0.963690	0.960247	0.956869	0.950288	0.943931	0.937791	0.931853	0.926111
4	0.971479	0.967761	0.964171	0.960688	0.957279	0.950648	0.944255	0.938086	0.932127	0.926365
5	0.972276	0.968458	0.964795	0.961256	0.957801	0.951100	0.944655	0.938446	0.932455	0.926668
6	0.973227	0.969278	0.965519	0.961908	0.958393	0.951605	0.945097	0.938839	0.932810	0.926993
7	0.974359	0.970236	0.966356	0.962653	0.959067	0.952171	0.945586	0.939272	0.933197	0.927344
8	0.975701	0.971352	0.967318	0.963502	0.959828	0.952804	0.946129	0.939746	0.933620	0.927724
9	0.979222	0.974161	0.969683	0.965556	0.961649	0.954291	0.947386	0.940837	0.934582	0.928585
10	0.984607	0.978027	0.972782	0.968173	0.963924	0.956104	0.948897	0.942131	0.935713	0.929588
11	1.000000	0.983798	0.976946	0.971524	0.966758	0.958292	0.950685	0.943644	0.937022	0.930741
12	0.983798	1.000000	0.983065	0.975957	0.970330	0.960924	0.952787	0.945396	0.938524	0.932053
13	0.976946	0.983065	1.000000	0.982391	0.974997	0.964112	0.955256	0.947418	0.940237	0.933537
14	0.971524	0.975957	0.982391	1.000000	0.981706	0.968047	0.958166	0.949748	0.942183	0.935206
15	0.966758	0.970330	0.974997	0.981706	1.000000	0.973145	0.961664	0.952465	0.944414	0.937099
16	0.958292	0.960924	0.964112	0.968047	0.973145	1.000000	0.971490	0.959461	0.949938	0.941682
17	0.950685	0.952787	0.955256	0.958166	0.961664	0.971490	1.000000	0.969994	0.957452	0.947626
18	0.943644	0.945396	0.947418	0.949748	0.952465	0.959461	0.969994	1.000000	0.968619	0.955601
19	0.937022	0.938524	0.940237	0.942183	0.944414	0.949938	0.957452	0.968619	1.000000	0.967349
20	0.930741	0.932053	0.933537	0.935206	0.937099	0.941682	0.947626	0.955601	0.967349	1.000000
21	0.923289	0.924419	0.925688	0.927103	0.928692	0.932472	0.937213	0.943222	0.951089	0.962200
22	0.916220	0.917211	0.918315	0.919540	0.920906	0.924116	0.928060	0.932910	0.938951	0.946699
23	0.903050	0.903840	0.904711	0.905668	0.906727	0.909175	0.912112	0.915605	0.919763	0.924737
24	0.890975	0.891626	0.892340	0.893118	0.893973	0.895934	0.898250	0.900958	0.904110	0.907774
25	0.879827	0.880378	0.880979	0.881629	0.882340	0.883960	0.885855	0.888045	0.890561	0.893437
26	0.869491	0.869966	0.870481	0.871036	0.871640	0.873009	0.874598	0.876420	0.878494	0.880841
27	0.859876	0.860292	0.860741	0.861221	0.861743	0.862920	0.864277	0.865825	0.867573	0.869537
28	0.842524	0.842855	0.843206	0.843581	0.843986	0.844889	0.845922	0.847088	0.848392	0.849841
29	0.827190	0.827461	0.827747	0.828050	0.828375	0.829095	0.829912	0.830826	0.831841	0.832962
30	0.813572	0.813800	0.814039	0.814290	0.814558	0.815148	0.815813	0.816552	0.817369	0.818263
31	0.801418	0.801614	0.801818	0.802030	0.802256	0.802751	0.803305	0.803917	0.804589	0.805323
32	0.790515	0.790687	0.790864	0.791047	0.791241	0.791665	0.792135	0.792651	0.793216	0.793830
33	0.771753	0.771890	0.772030	0.772173	0.772323	0.772646	0.773002	0.773390	0.773809	0.774261
34	0.756160	0.756274	0.756389	0.756506	0.756627	0.756888	0.757171	0.757477	0.757806	0.758157
35	0.742907	0.743005	0.743103	0.743202	0.743304	0.743522	0.743757	0.744008	0.744277	0.744562
36	0.731400	0.731487	0.731573	0.731659	0.731747	0.731935	0.732135	0.732349	0.732575	0.732815
37	0.721214	0.721292	0.721369	0.721446	0.721524	0.721689	0.721865	0.722051	0.722247	0.722453
38	0.709889	0.709959	0.710027	0.710094	0.710164	0.710308	0.710460	0.710621	0.710790	0.710966
39	0.699406	0.699469	0.699531	0.699591	0.699653	0.699781	0.699916	0.700057	0.700204	0.700359
40	0.679307	0.679360	0.679410	0.679460	0.679510	0.679614	0.679721	0.679833	0.679949	0.680069
41	0.660297	0.660341	0.660384	0.660425	0.660466	0.660551	0.660639	0.660729	0.660822	0.660918
42	0.642466	0.642503	0.642539	0.642574	0.642608	0.642679	0.642752	0.642826	0.642902	0.642981
43	0.625825	0.625858	0.625888	0.625918	0.625947	0.626007	0.626068	0.626130	0.626193	0.626258
44	0.610337	0.610365	0.610392	0.610417	0.610442	0.610493	0.610545	0.610598	0.610651	0.610705
45	0.595871	0.595895	0.595918	0.595940	0.595962	0.596006	0.596051	0.596095	0.596141	0.596187
46	0.582345	0.582367	0.582387	0.582406	0.582425	0.582463	0.582502	0.582541	0.582580	0.582619
47	0.569689	0.569708	0.569726	0.569742	0.569759	0.569793	0.569826	0.569860	0.569893	0.569928
48	0.557835	0.557851	0.557867	0.557882	0.557897	0.557926	0.557955	0.557985	0.558014	0.558044
49	0.546723	0.546738	0.546752	0.546766	0.546779	0.546804	0.546830	0.546856	0.546882	0.546908
50	0.536301	0.536314	0.536327	0.536338	0.536350	0.536373	0.536396	0.536419	0.536442	0.536465
51	0.526500	0.526512	0.526523	0.526533	0.526544	0.526564	0.526585	0.526605	0.526625	0.526646
52	0.517264	0.517275	0.517285	0.517294	0.517303	0.517322	0.517340	0.517358	0.517376	0.517394
53	0.508548	0.508558	0.508567	0.508575	0.508584	0.508600	0.508617	0.508633	0.508649	0.508665
54	0.500311	0.500320	0.500328	0.500336	0.500343	0.500359	0.500373	0.500388	0.500402	0.500417
55	0.498203	0.498212	0.498220	0.498227	0.498235	0.498249	0.498264	0.498278	0.498292	0.498306
56	0.492511	0.492520	0.492527	0.492534	0.492541	0.492555	0.492568	0.492581	0.492594	0.492607
57	0.485112	0.485119	0.485126	0.485133	0.485139	0.485151	0.485163	0.485175	0.485187	0.485199

man and Benedict [1978]. Considerable experimental uncertainties exist in the specification of both band intensities and line widths. For intensities, these occur because of the difficulty of apportioning exactly the intensities derived from many bands into separate contributions from each CO₂ band. For line widths the most recent available measurements made with laser diodes have fractional experimental errors of ±5 to 10%. To complicate further the situation, errors in absorptivity are, in general, a function of each error (i.e., in the strong-line approximation, the fractional absorptivity error = half (the fractional error in intensity + the fractional error in line width)).

To test the effect of these uncertainties on our results, we first obtain transmittances calculated by using the line-by-line program, using the values of line intensities and half-widths given by Drayson [1973] (Table 8). The temperature sounding

is the mid-latitude profile T₀ given in Table 1. In Table 9 we present the fractional change in absorption owing to the use of Drayson line intensities, that is

$$\frac{a_{\text{Drayson}} - a_{\text{AFGL}}}{a_{\text{AFGL}}}$$

We observe that the fractional absorption, using the Drayson values, has decreased in the upper stratosphere and mesosphere, by up to 2.5 percent at 7 mbar. No change in absorption from the top of the atmosphere to the surface is apparent, and a small decrease in absorption in tropospheric levels is obtained.

These results may be understood by noting that the AFGL band intensity for the fundamental (01101 – 00001) band is about 0.3% less than that of Drayson; furthermore, the AGFL intensities for the first hot bands (bands 2–4 in Table 8), taken

TABLE 6. (continued)

	21	22	23	24	25	26	27	28	29	30
1	0.919070	0.912431	0.899988	0.888274	0.877463	0.867387	0.857979	0.840935	0.825820	0.812364
2	0.919110	0.912468	0.899932	0.888304	0.877491	0.867413	0.858003	0.840956	0.825841	0.812384
3	0.919192	0.912545	0.900001	0.888368	0.877549	0.867468	0.858055	0.841003	0.825883	0.812423
4	0.919427	0.912763	0.900195	0.888543	0.877711	0.867617	0.858195	0.841128	0.825997	0.812528
5	0.919703	0.913019	0.900419	0.888743	0.877892	0.867784	0.858349	0.841264	0.826119	0.812640
6	0.919997	0.913287	0.900648	0.888945	0.878073	0.867948	0.858500	0.841395	0.826235	0.812743
7	0.920311	0.913572	0.900889	0.889154	0.878258	0.868115	0.858652	0.841524	0.826347	0.812844
8	0.920650	0.913878	0.901145	0.889373	0.878451	0.868286	0.858807	0.841654	0.826460	0.812944
9	0.921410	0.914558	0.901706	0.889851	0.878866	0.868654	0.859135	0.841926	0.826692	0.813146
10	0.922288	0.915338	0.902340	0.890383	0.879324	0.869054	0.859491	0.842216	0.826935	0.813354
11	0.923289	0.916220	0.903050	0.890975	0.879827	0.869491	0.859876	0.842524	0.827190	0.813572
12	0.924419	0.917211	0.903840	0.891626	0.880378	0.869966	0.860292	0.842855	0.827461	0.813800
13	0.925688	0.918315	0.904711	0.892340	0.880979	0.870481	0.860741	0.843206	0.827747	0.814039
14	0.927103	0.919540	0.905668	0.893118	0.881629	0.871036	0.861221	0.843581	0.828050	0.814290
15	0.928692	0.920906	0.906727	0.893973	0.882340	0.871640	0.861743	0.843986	0.828375	0.814558
16	0.932472	0.924116	0.909175	0.895934	0.883960	0.873009	0.862920	0.844889	0.829095	0.815148
17	0.937213	0.928060	0.912112	0.898250	0.885855	0.874598	0.864277	0.845922	0.829912	0.815813
18	0.943222	0.932910	0.915605	0.900958	0.888045	0.876420	0.865825	0.847088	0.830826	0.816552
19	0.951089	0.938951	0.919763	0.904110	0.890561	0.878494	0.867573	0.848392	0.831841	0.817369
20	0.962200	0.946699	0.924737	0.907774	0.893437	0.880841	0.869537	0.849841	0.832962	0.818263
21	1.000000	0.960675	0.932480	0.913221	0.897616	0.884200	0.872322	0.851870	0.834515	0.819495
22	0.960675	1.000000	0.942775	0.919897	0.902563	0.888101	0.875513	0.854157	0.836249	0.820860
23	0.932480	0.942775	1.000000	0.939336	0.915633	0.897952	0.883360	0.859608	0.840306	0.824013
24	0.913221	0.919897	0.939336	1.000000	0.936268	0.911815	0.893811	0.866473	0.845266	0.827792
25	0.897616	0.902563	0.915633	0.936268	1.000000	0.933491	0.908352	0.875204	0.851325	0.832302
26	0.884200	0.888101	0.897952	0.911815	0.933491	1.000000	0.930953	0.886592	0.858784	0.837687
27	0.872322	0.875513	0.883360	0.893811	0.908352	0.930953	1.000000	0.902244	0.868126	0.844156
28	0.851870	0.854157	0.859608	0.866473	0.875204	0.886592	0.902244	1.000000	0.896665	0.861803
29	0.834515	0.836249	0.840306	0.845266	0.851325	0.858784	0.868126	0.896665	1.000000	0.891744
30	0.819495	0.820860	0.824013	0.827792	0.832302	0.837687	0.844156	0.861803	0.891744	1.000000
31	0.806327	0.807431	0.809958	0.812945	0.816451	0.820555	0.825367	0.837793	0.856236	0.887342
32	0.794666	0.795581	0.797655	0.800082	0.802893	0.806138	0.809879	0.819219	0.832189	0.851266
33	0.774871	0.775533	0.777015	0.778716	0.780652	0.782843	0.785312	0.791224	0.798873	0.808936
34	0.758628	0.759135	0.760259	0.761531	0.762959	0.764552	0.766321	0.770449	0.775584	0.781994
35	0.744942	0.745349	0.746241	0.747241	0.748351	0.749576	0.750921	0.754002	0.757740	0.762259
36	0.733133	0.733470	0.734206	0.735023	0.735922	0.736905	0.737976	0.740395	0.743277	0.746687
37	0.722726	0.723015	0.723639	0.724328	0.725079	0.725896	0.726779	0.728753	0.731075	0.733779
38	0.711199	0.711443	0.711968	0.712542	0.713165	0.713836	0.714558	0.716154	0.718008	0.720138
39	0.700560	0.700771	0.701223	0.701713	0.702241	0.702807	0.703412	0.704740	0.706268	0.708007
40	0.680225	0.680387	0.680730	0.681099	0.681492	0.681910	0.682352	0.683311	0.684399	0.685620
41	0.661042	0.661170	0.661439	0.661725	0.662027	0.662346	0.662681	0.663401	0.664209	0.665106
42	0.643081	0.643184	0.643400	0.643627	0.643865	0.644115	0.644376	0.644933	0.645552	0.646234
43	0.626341	0.626426	0.626602	0.626786	0.626978	0.627178	0.627386	0.627827	0.628314	0.628847
44	0.610775	0.610846	0.610991	0.611143	0.611301	0.611464	0.611633	0.611990	0.612381	0.612807
45	0.596246	0.596306	0.596428	0.596555	0.596686	0.596821	0.596961	0.597254	0.597573	0.597919
46	0.582669	0.582720	0.582824	0.582932	0.583042	0.583156	0.583272	0.583516	0.583780	0.584066
47	0.569971	0.570015	0.570104	0.570195	0.570289	0.570385	0.570484	0.570689	0.570910	0.571148
48	0.558082	0.558119	0.558196	0.558275	0.558355	0.558438	0.558522	0.558695	0.558883	0.559083
49	0.546941	0.546974	0.547041	0.547109	0.547178	0.547249	0.547321	0.547470	0.547629	0.547800
50	0.536493	0.536522	0.536581	0.536640	0.536700	0.536762	0.536824	0.536952	0.537089	0.537235
51	0.526671	0.526697	0.526748	0.526800	0.526853	0.526906	0.526960	0.527071	0.527189	0.527315
52	0.517417	0.517440	0.517485	0.517531	0.517577	0.517624	0.517671	0.517768	0.517871	0.517980
53	0.508685	0.508706	0.508746	0.508786	0.508827	0.508868	0.508910	0.508995	0.509085	0.509179
54	0.500435	0.500453	0.500489	0.500525	0.500561	0.500598	0.500635	0.500709	0.500788	0.500871
55	0.498324	0.498341	0.498376	0.498411	0.498446	0.498482	0.498517	0.498590	0.498666	0.498746
56	0.492624	0.492640	0.492672	0.492705	0.492737	0.492769	0.492802	0.492868	0.492938	0.493011
57	0.485214	0.485229	0.485258	0.485287	0.485316	0.485345	0.485374	0.485433	0.485495	0.485560

together, are also slightly less than those of Drayson. The remaining differences are to be found in the line broadening coefficients; an examination of the coefficients for the individual lines of the fundamental band indicates that the AFGL coefficients exceed those of Drayson for most lines and that for the strongest lines the fractional difference is about 4%.

A similar difference may be obtained by examining the lines of the strong lines of other bands. For the region of the upper stratosphere and mesosphere, we may assume that absorption is dominated by the fundamental band and that the strong-line approximation is a reasonable representation of the actual absorption. In that case the actual fractional change in absorption shown in Table 9 is closely simulated by the fractional difference computed from the change in line intensities and in line broadening coefficients.

We next consider the recent line intensity and line width

measurements made by Planet and coworkers [Planet et al., 1978; Planet and Tettener, 1979; Tettener and Planet, 1980]. In this work, intensities and widths of individual lines of the Q and R branches of the fundamental and of the 02201 – 01101 band were measured by using a tunable laser diode with resolution of $\sim 10^{-4}$ cm $^{-1}$. A comparison of their fitted results with those of AFGL is shown in Table 10, using the results for the fundamental band given in Planet and Tettener [1979]. We observe that their measurement of line intensities is about 4% lower than the value given in AFGL; on the other hand, the measured line widths are about 10% higher than that of AFGL. Again making the strong-line approximation, we find that the use of Planet's values would cause the fractional absorption to increase by 3%. It should be noted, however, that error bars of 5–10% are quoted in both line intensities and line widths [see Planet and Tettener, 1979, Tables 2a–2b].

TABLE 6. (continued)

	31	32	33	34	35	36	37	38	39	40
1	0.800337	0.789533	0.770917	0.755425	0.742246	0.730795	0.720653	0.709373	0.698927	0.678893
2	0.800354	0.789550	0.770933	0.755439	0.742259	0.730807	0.720665	0.709384	0.698937	0.678902
3	0.800391	0.789584	0.770564	0.755468	0.742286	0.730832	0.720689	0.709406	0.698959	0.678921
4	0.800489	0.789676	0.771046	0.755543	0.742356	0.730898	0.720751	0.709464	0.699013	0.678970
5	0.800592	0.789772	0.771131	0.755620	0.742427	0.730964	0.720813	0.709523	0.699068	0.679018
6	0.800686	0.789860	0.771208	0.755689	0.742489	0.731022	0.720868	0.709573	0.699115	0.679059
7	0.800777	0.789943	0.771280	0.755753	0.742548	0.731076	0.720917	0.709619	0.699158	0.679097
8	0.800867	0.790024	0.771349	0.755814	0.742602	0.731126	0.720964	0.709662	0.699198	0.679131
9	0.801046	0.790186	0.771484	0.755931	0.742707	0.731221	0.721051	0.709742	0.699272	0.679194
10	0.801229	0.790348	0.771619	0.756046	0.742808	0.731312	0.721134	0.709817	0.699340	0.679252
11	0.801418	0.790515	0.771753	0.756160	0.742907	0.731400	0.721214	0.709889	0.699406	0.679307
12	0.801614	0.790687	0.771890	0.756274	0.743005	0.731487	0.721292	0.709959	0.699469	0.679360
13	0.801818	0.790864	0.772030	0.756389	0.743103	0.731573	0.721369	0.710027	0.699531	0.679410
14	0.802030	0.791047	0.772173	0.756506	0.743202	0.731659	0.721446	0.710094	0.699591	0.679460
15	0.802256	0.791241	0.772323	0.756627	0.743304	0.731747	0.721524	0.710164	0.699653	0.679510
16	0.802751	0.791665	0.772646	0.756888	0.743522	0.731935	0.721689	0.710308	0.699781	0.679614
17	0.803305	0.792135	0.773002	0.757171	0.743757	0.732135	0.721865	0.710460	0.699916	0.679721
18	0.803917	0.792651	0.773390	0.757477	0.744008	0.732349	0.722051	0.710621	0.700057	0.679833
19	0.804589	0.793216	0.773809	0.757806	0.744277	0.732575	0.722247	0.710790	0.700204	0.679949
20	0.805323	0.793830	0.774261	0.758157	0.744562	0.732815	0.722453	0.710966	0.700359	0.680069
21	0.806327	0.794666	0.774871	0.758628	0.744942	0.733133	0.722726	0.711199	0.700560	0.680225
22	0.807431	0.795581	0.775533	0.759135	0.745349	0.733470	0.723015	0.711443	0.700771	0.680387
23	0.809958	0.797655	0.777015	0.760259	0.746241	0.734206	0.723639	0.711968	0.701223	0.680730
24	0.812945	0.800082	0.778716	0.761531	0.747241	0.735023	0.724328	0.712542	0.701713	0.681099
25	0.816451	0.802893	0.780652	0.762959	0.748351	0.735922	0.725079	0.713165	0.702241	0.681492
26	0.820555	0.806138	0.782843	0.764552	0.749576	0.736905	0.725896	0.713836	0.702807	0.681910
27	0.825367	0.809879	0.785312	0.766321	0.750921	0.737976	0.726779	0.714558	0.703412	0.682352
28	0.837793	0.819219	0.791224	0.770449	0.754002	0.740395	0.728753	0.716154	0.704740	0.683311
29	0.856236	0.832189	0.798873	0.775584	0.757740	0.743277	0.731075	0.718008	0.706268	0.684399
30	0.887342	0.851266	0.808936	0.781994	0.762259	0.746687	0.733779	0.720138	0.708007	0.685620
31	1.000000	0.883360	0.822653	0.790097	0.767741	0.750717	0.736918	0.722572	0.709971	0.686978
32	0.883360	1.000000	0.842652	0.800598	0.774461	0.755496	0.740559	0.725344	0.712180	0.688480
33	0.822653	0.842652	1.000000	0.835464	0.793654	0.768152	0.749770	0.732108	0.717446	0.691961
34	0.790097	0.800598	0.835464	1.000000	0.829305	0.787730	0.762743	0.741007	0.724094	0.696155
35	0.767741	0.774461	0.793654	0.829305	1.000000	0.823939	0.782591	0.753160	0.732625	0.701205
36	0.750717	0.755496	0.768152	0.787730	0.823939	1.000000	0.819205	0.771044	0.743964	0.707328
37	0.736918	0.740559	0.749770	0.762743	0.782591	0.819205	1.000000	0.801845	0.760073	0.714870
38	0.722572	0.725344	0.732108	0.741007	0.753160	0.771044	0.801845	1.000000	0.795919	0.727249
39	0.709971	0.712180	0.717446	0.724094	0.732625	0.743964	0.760073	0.795919	1.000000	0.746138
40	0.686978	0.688480	0.691961	0.696155	0.701205	0.707328	0.714870	0.727249	0.746138	1.000000
41	0.666694	0.667176	0.669640	0.672532	0.675908	0.679841	0.684435	0.691344	0.700373	0.733136
42	0.646979	0.647790	0.649613	0.651719	0.654130	0.656878	0.660004	0.664529	0.670121	0.687226
43	0.629426	0.630052	0.631447	0.633040	0.634841	0.636864	0.639130	0.642339	0.646197	0.657250
44	0.613267	0.613762	0.614859	0.616099	0.617489	0.619035	0.620747	0.623140	0.625970	0.633810
45	0.598292	0.598692	0.599571	0.600558	0.601657	0.602870	0.604203	0.606049	0.608209	0.614074
46	0.584372	0.584699	0.585416	0.586216	0.587100	0.588072	0.589133	0.590592	0.592287	0.596832
47	0.571403	0.571674	0.572266	0.572923	0.573646	0.574436	0.575296	0.576470	0.577828	0.581438
48	0.559297	0.559524	0.560018	0.560564	0.561162	0.561813	0.562518	0.563477	0.564582	0.567502
49	0.547981	0.548173	0.548589	0.549046	0.549546	0.550088	0.550673	0.551465	0.552375	0.554771
50	0.537389	0.537553	0.537906	0.538292	0.538713	0.539168	0.539658	0.540319	0.541076	0.543064
51	0.527448	0.527588	0.527889	0.528219	0.528576	0.528961	0.529373	0.529929	0.530564	0.532229
52	0.518094	0.518215	0.518474	0.518756	0.519061	0.519389	0.519739	0.520210	0.520746	0.522151
53	0.509279	0.509384	0.509608	0.509851	0.510113	0.510394	0.510693	0.511094	0.511550	0.512744
54	0.500959	0.501050	0.501245	0.501455	0.501682	0.501924	0.502181	0.502525	0.502915	0.503936
55	0.498831	0.498919	0.499107	0.499310	0.499528	0.499761	0.500008	0.500338	0.500713	0.501694
56	0.493088	0.493168	0.493338	0.493522	0.493719	0.493929	0.494151	0.494447	0.494783	0.495663
57	0.485628	0.485698	0.485848	0.486009	0.486181	0.486364	0.486557	0.486814	0.487105	0.487867

As a final test of the validity of our use of the AFGL line parameters, we have compared our results with a series of measurements on the 15-μm band recently made by Burch and coworkers [Gryvnak *et al.*, 1976; Gryvnak and Burch, 1978]. In these comparisons, details of which will be reported on in a later paper, we have used the line-by-line method to calculate integrated absorptivities for 24 samples corresponding exactly to experimental conditions given in the Gryvnak and Burch report. We find that the average fractional error (using a cutoff of $\nu_c = 3 \text{ cm}^{-1}$) for the line-by-line calculations is less than 0.4%. In view of the 1–2% uncertainties found above, there appears to be little undetected systematic error caused by the use of any of the above sets of line parameters. A comparison of these changes in absorption with the errors shown in Table 3a and 3b shows that the absorption differences are much smaller than the error in neglecting all tem-

perature effects. However, these errors are larger than those arising from differences in perturbation methods (Tables 3c–3h). We may conclude that the major remaining source of error in obtaining CO₂ transmittances is experimental uncertainty in the determination of line and band intensities and line profiles.

b. Comparison of Treatments of CO₂ Line Profiles and Temperature Effects

We next discuss the difference in our results from those of other workers owing to different representation of CO₂ line profiles and treatment of intensity variations along the optical path. To do this, we compare transmittances (or cooling rates derived from these transmittances) from the present work to those of previous investigators. Infrared cooling rates for the stratosphere or mesosphere,

TABLE 6. (continued)

	41	42	43	44	45	46	47	48	49	50
1	0.659936	0.642150	0.625548	0.610092	0.595653	0.582151	0.569515	0.557678	0.546582	0.536173
2	0.659945	0.642157	0.625554	0.610098	0.595658	0.582156	0.569519	0.557682	0.546586	0.536176
3	0.659961	0.642172	0.625568	0.610110	0.595669	0.582166	0.569528	0.557690	0.546593	0.536183
4	0.660005	0.642211	0.625602	0.610141	0.595697	0.582190	0.569551	0.557710	0.546612	0.536200
5	0.660048	0.642249	0.625636	0.610171	0.595723	0.582215	0.569572	0.557730	0.546629	0.536216
6	0.660084	0.642281	0.625664	0.610196	0.595746	0.582235	0.569590	0.557746	0.546644	0.536229
7	0.660116	0.642309	0.625689	0.610218	0.595766	0.582252	0.569606	0.557761	0.546657	0.536241
8	0.660146	0.642335	0.625712	0.610238	0.595784	0.582268	0.569621	0.557774	0.546669	0.536251
9	0.660201	0.642383	0.625754	0.610274	0.595816	0.582297	0.569646	0.557796	0.546689	0.536270
10	0.660251	0.642426	0.625791	0.610307	0.595845	0.582322	0.569668	0.557816	0.546707	0.536286
11	0.660297	0.642466	0.625825	0.610337	0.595871	0.582345	0.569689	0.557835	0.546723	0.536301
12	0.660341	0.642503	0.625858	0.610365	0.595895	0.582367	0.569708	0.557851	0.546738	0.536314
13	0.660384	0.642539	0.625888	0.610392	0.595918	0.582387	0.569726	0.557867	0.546752	0.536327
14	0.660425	0.642574	0.625918	0.610417	0.595940	0.582406	0.569742	0.557882	0.546766	0.536338
15	0.660466	0.642608	0.625947	0.610442	0.595962	0.582425	0.569759	0.557897	0.546779	0.536350
16	0.660551	0.642679	0.626007	0.610493	0.596006	0.582463	0.569793	0.557926	0.546804	0.536373
17	0.660639	0.642752	0.626068	0.610545	0.596051	0.582502	0.569826	0.557955	0.546830	0.536396
18	0.660729	0.642826	0.626130	0.610598	0.596095	0.582541	0.569860	0.557985	0.546856	0.536419
19	0.660822	0.642902	0.626193	0.610651	0.596141	0.582580	0.569893	0.558014	0.546882	0.536442
20	0.660918	0.642981	0.626258	0.610705	0.596187	0.582619	0.569928	0.558044	0.546908	0.536465
21	0.661042	0.643081	0.626341	0.610775	0.596246	0.582669	0.569971	0.558082	0.546941	0.536493
22	0.661170	0.643184	0.626426	0.610846	0.596306	0.582720	0.570015	0.558119	0.546974	0.536522
23	0.661439	0.643400	0.626602	0.610991	0.596428	0.582824	0.570104	0.558196	0.547041	0.536581
24	0.661725	0.643627	0.626786	0.611143	0.596555	0.582932	0.570195	0.558275	0.547109	0.536640
25	0.662027	0.643865	0.626978	0.611301	0.596686	0.583042	0.570289	0.558355	0.547178	0.536700
26	0.662346	0.644115	0.627178	0.611464	0.596821	0.583156	0.570385	0.558438	0.547249	0.536762
27	0.662681	0.644376	0.627386	0.611633	0.596961	0.583272	0.570484	0.558522	0.547321	0.536824
28	0.663401	0.644933	0.627827	0.611990	0.597254	0.583516	0.570689	0.558695	0.547470	0.536952
29	0.664209	0.645552	0.628314	0.612381	0.597573	0.583780	0.570910	0.558883	0.547629	0.537089
30	0.665106	0.646234	0.628847	0.612807	0.597919	0.584066	0.571148	0.559083	0.547800	0.537235
31	0.666094	0.646979	0.629426	0.613267	0.598292	0.584372	0.571403	0.559297	0.547981	0.537389
32	0.667176	0.647790	0.630052	0.613762	0.598692	0.584699	0.571674	0.559524	0.548173	0.537553
33	0.669640	0.649613	0.631447	0.614859	0.599571	0.585416	0.572266	0.560018	0.548589	0.537906
34	0.672532	0.651719	0.633040	0.616099	0.600558	0.586216	0.572923	0.560564	0.549046	0.538292
35	0.675908	0.654130	0.634841	0.617489	0.601657	0.587100	0.573646	0.561162	0.549546	0.538713
36	0.679841	0.656878	0.636864	0.619035	0.602870	0.588072	0.574436	0.561813	0.550088	0.539168
37	0.684435	0.660004	0.639130	0.620747	0.604203	0.589133	0.575296	0.562518	0.550673	0.539658
38	0.691344	0.664529	0.642339	0.623140	0.606049	0.590592	0.576470	0.563477	0.551465	0.540319
39	0.700373	0.670121	0.646197	0.625970	0.608209	0.592287	0.577828	0.564582	0.552375	0.541076
40	0.733136	0.687226	0.657250	0.633810	0.614074	0.596832	0.581438	0.567502	0.554771	0.543064
41	1.000000	0.721795	0.675679	0.645901	0.622751	0.603390	0.586564	0.571605	0.558112	0.545822
42	0.721795	0.1000000	0.711791	0.665450	0.635706	0.612769	0.593707	0.577225	0.562637	0.549526
43	0.675679	0.711791	1.000000	0.702899	0.656180	0.626440	0.603671	0.584859	0.568674	0.554409
44	0.645901	0.665450	0.702899	1.000000	0.694692	0.647657	0.617925	0.595303	0.576712	0.560793
45	0.622751	0.635706	0.656180	0.694692	1.000000	0.687179	0.639839	0.610100	0.587601	0.569204
46	0.603390	0.612769	0.626440	0.647657	0.687179	1.000000	0.680277	0.632637	0.602882	0.580488
47	0.586564	0.593707	0.603671	0.617925	0.639839	0.680277	1.000000	0.673904	0.625977	0.596198
48	0.571605	0.577225	0.584859	0.595303	0.610100	0.632637	0.673904	1.000000	0.668007	0.619801
49	0.558112	0.562637	0.568674	0.576712	0.587601	0.602882	0.625977	0.668007	1.000000	0.662531
50	0.545822	0.549526	0.554409	0.560793	0.569204	0.580488	0.596198	0.619801	0.662531	1.000000
51	0.534530	0.537602	0.541617	0.546798	0.553498	0.562237	0.573866	0.589956	0.614004	0.657341
52	0.524088	0.526663	0.530005	0.534278	0.539731	0.546709	0.555732	0.567660	0.584077	0.608505
53	0.514388	0.516565	0.519377	0.522946	0.527456	0.533147	0.540364	0.549633	0.561818	0.578513
54	0.505340	0.507196	0.509583	0.512596	0.516375	0.521093	0.526992	0.534416	0.543895	0.556296
55	0.503042	0.504823	0.507112	0.509998	0.513610	0.518110	0.523717	0.530745	0.539663	0.551225
56	0.496870	0.498463	0.500507	0.503074	0.506273	0.510237	0.515137	0.521215	0.528817	0.538472
57	0.488912	0.490290	0.492051	0.494257	0.496993	0.500359	0.504485	0.509545	0.515777	0.523529

first calculated by Plass [1956] and Murgatroyd and Goody [1958], have subsequently been obtained by many workers. However, the two results which are most directly comparable to ours are those of Plass [1963] and Dickinson [1972, 1973].

Plass [1963] has calculated transmittances from the top of the atmosphere to selected heights in the stratosphere for a standard temperature profile [U.S. Air Force, 1960], using a quasi-random model of the 15-μm (and other) CO₂ bands. His results are suitable for comparison with ours because (1) the calculations are performed at 2.5 cm⁻¹ intervals, then consolidated to 50 cm⁻¹ intervals, thus making it easy to compare with our results calculated in 50 cm⁻¹ intervals; (2) the mixing ratio for CO₂ employed is the same as ours, 330 ppmv; (3) Plass has calculated transmittances for slant paths ranging from 0° to 90°, thus affording easy comparison with our angularly integrated transmittances.

In Table 11 we present a comparison of equivalent widths for the 15-μm band derived from Plass for atmospheric heights of 15, 25, 30 and 50 km with those obtained by the present program using pressure interpolation. It should be noted that the band interval for the Plass result extends from 550 to 900 cm⁻¹, whereas ours extends from 500 to 850 cm⁻¹. This may explain, in part, the somewhat higher equivalent widths found in our work. Also, Plass employs the Benedict modification of the Lorentz line profile in his calculation [Plass, 1964], whereas we use the cutoff Voigt profile. In general we see close correspondence (within 5%) in the results at 15 and 25 km. At higher levels the disagreement is relatively large, indicating that the CO₂ line shapes at these altitudes require a Voigt profile for a proper description.

Dickinson [1972, 1973] has calculated CO₂ cooling rates for the 30–70 km region. Briefly, his method consists of calcu-

TABLE 6. (continued)

	51	52	53	54	55	56	57
1	0.526384	0.517158	0.508451	0.500222	0.498116	0.492429	0.485036
2	0.526386	0.517161	0.508453	0.500224	0.498118	0.492431	0.485038
3	0.526393	0.517166	0.508459	0.500229	0.498123	0.492436	0.485042
4	0.526408	0.517180	0.508472	0.500241	0.498134	0.492447	0.485052
5	0.526423	0.517194	0.508484	0.500252	0.498146	0.492458	0.485062
6	0.526435	0.517205	0.508494	0.500262	0.498155	0.492466	0.485070
7	0.526446	0.517215	0.508503	0.500270	0.498163	0.492474	0.485077
8	0.526455	0.517223	0.508511	0.500277	0.498170	0.492481	0.485083
9	0.526472	0.517239	0.508525	0.500290	0.498182	0.492492	0.485094
10	0.526487	0.517252	0.508537	0.500301	0.498193	0.492502	0.485103
11	0.526500	0.517264	0.508548	0.500311	0.498203	0.492511	0.485112
12	0.526512	0.517275	0.508558	0.500320	0.498212	0.492520	0.485119
13	0.526523	0.517285	0.508567	0.500328	0.498220	0.492527	0.485126
14	0.526533	0.517294	0.508575	0.500336	0.498227	0.492534	0.485133
15	0.526544	0.517303	0.508584	0.500343	0.498235	0.492541	0.485139
16	0.526564	0.517322	0.508600	0.500359	0.498249	0.492555	0.485151
17	0.526585	0.517340	0.508617	0.500373	0.498264	0.492568	0.485163
18	0.526605	0.517358	0.508633	0.500388	0.498278	0.492581	0.485175
19	0.526625	0.517376	0.508649	0.500402	0.498292	0.492594	0.485187
20	0.526646	0.517394	0.508665	0.500417	0.498306	0.492607	0.485199
21	0.526671	0.517417	0.508685	0.500435	0.498324	0.492624	0.485214
22	0.526697	0.517440	0.508706	0.500453	0.498341	0.492640	0.485229
23	0.526748	0.517485	0.508746	0.500489	0.498376	0.492672	0.485258
24	0.526800	0.517531	0.508786	0.500525	0.498411	0.492705	0.485287
25	0.526853	0.517577	0.508827	0.500561	0.498446	0.492737	0.485316
26	0.526906	0.517624	0.508868	0.500598	0.498482	0.492769	0.485345
27	0.526960	0.517671	0.508910	0.500635	0.498517	0.492802	0.485374
28	0.527071	0.517768	0.508995	0.500709	0.498590	0.492868	0.485433
29	0.527189	0.517871	0.509085	0.500788	0.498666	0.492938	0.485495
30	0.527315	0.517980	0.509179	0.500871	0.498746	0.493011	0.485560
31	0.527448	0.518094	0.509279	0.500959	0.498831	0.493088	0.485628
32	0.527588	0.518215	0.509384	0.501050	0.498919	0.493168	0.485698
33	0.527889	0.518474	0.509608	0.501245	0.499107	0.493338	0.485848
34	0.528219	0.518756	0.509851	0.501455	0.499310	0.493522	0.486009
35	0.528576	0.519061	0.510113	0.501682	0.499528	0.493719	0.486181
36	0.528961	0.519389	0.510394	0.501924	0.499761	0.493929	0.486364
37	0.529373	0.519739	0.510693	0.502181	0.500008	0.494151	0.486557
38	0.529929	0.520210	0.511094	0.502525	0.500338	0.494447	0.486814
39	0.530564	0.520746	0.511550	0.502915	0.500713	0.494783	0.487105
40	0.532229	0.522151	0.512744	0.503936	0.501694	0.495663	0.487867
41	0.534530	0.524088	0.514388	0.505340	0.503042	0.496870	0.488912
42	0.537602	0.526663	0.516565	0.507196	0.504823	0.498463	0.490290
43	0.541617	0.530005	0.519377	0.509583	0.507112	0.500507	0.492051
44	0.546798	0.534278	0.522946	0.512596	0.509998	0.503074	0.494257
45	0.553498	0.539731	0.527456	0.516375	0.513610	0.506273	0.496993
46	0.562237	0.546709	0.533147	0.521093	0.518110	0.510237	0.500359
47	0.573866	0.555732	0.540364	0.526992	0.523717	0.515137	0.504485
48	0.589956	0.567660	0.549633	0.534416	0.530745	0.521215	0.509545
49	0.614004	0.584077	0.561818	0.543895	0.539663	0.528817	0.515777
50	0.657341	0.608505	0.578513	0.556296	0.551225	0.538472	0.523529
51	1.000000	0.652420	0.603301	0.573253	0.566806	0.551076	0.533348
52	0.652420	1.000000	0.647777	0.598387	0.589274	0.568280	0.546141
53	0.603301	0.647777	1.000000	0.643395	0.626662	0.593733	0.563568
54	0.573253	0.598387	0.643395	1.000000	0.735200	0.638999	0.589313
55	0.566806	0.589274	0.626662	0.735200	1.000000	0.660103	0.598559
56	0.551076	0.568280	0.593733	0.638999	0.660103	1.000000	0.635287
57	0.533348	0.546141	0.563568	0.589313	0.598559	0.635287	1.000000

lating individual line positions and strengths from the 15-μm band intensities and centers, using a harmonic vibrator-rotator approximation. To save computer time, lines within bands are partitioned into groups on the basis of strength, and then each group is treated as one equivalent line. Voigt effects are included in the treatment of the lines; however, the variation of line intensity along the optical path is only approximated. Line overlap is crudely parameterized by using the method of Goody and Belton [1967]. This calculation serves as a benchmark for the subsequent Newtonian cooling approximation, whose accuracy we have referred to in section 1d.

We have compared cooling rates obtained by using Dickinson's method and by the present method. To do this, transmission functions were obtained for individual bands (and isotopes) using Drayson's catalogue and the line-by-line method. From these, cooling rates were computed, and these were

compared with Dickinson's results for the corresponding band and isotope. In Table 12 we present the result of such a comparison for the C¹²O₂¹⁶ fundamental band, for the total fundamental band (all isotopes), for the first and second hot band groups (bands 2–4 and bands 5 and 9), and for all bands. It should be noted that (1) both results employ the same CO₂ mixing ratio, and (2) Dickinson's band intensities and line widths have been adjusted to be the same as Drayson's. The most striking part of the comparison is the rather close agreement between the two models for the fundamental C¹²O₂¹⁶ band and the rather large differences in the second hot band at 49.5 and 53 km. We have invested considerable effort in eliminating inconsistencies between the two calculations. We believe that the remaining differences may be due to the approximation used by Dickinson in handling line overlap and perhaps to the method he employs for accounting for the tem-

perature variation of line intensity along the path. It should be noted, however, that these differences are much smaller in magnitude than those reported comparing Dickinson's work to previous results.

5. CONCLUSION

a. Future Improvements in the Tables

The algorithm we have presented in this paper may be fairly called both fast and accurate, but this does not mean that further improvement is not desirable and possible. As was previously pointed out, the fundamental spectroscopic data on which the table are based is not as well known as we should like. At such time as demonstrably better intensities or widths become available, it is our intention to recalculate the tables and to publish revised versions.

There are several other possible modifications which may be important. The AFGL compilation lists on the order of 20,000 lines in the CO₂ 15-μm band complex; of these, only 3,800 are included in our computation. To assess the effects the exclusion of the many very weak lines, we are developing correction methods based on the Goody random model and the approximations for Voigt lines discussed by Fels [1979]. Preliminary results suggest that neglect of the weak lines may result in an underestimate of absorption of up to 1%. We hope to report on this in the near future.

In addition to the above problem, there is the more vexing one having to do with the true shape of CO₂ 15 μm lines. Our calculations assume that non-Lorentzian effects do not modify the line shape within 3 cm⁻¹ of the center and abruptly cut off the line beyond this. Although this gives very good agreement

TABLE 7. Band Parameters Used in the Line-by-Line Program
[After Rothman and Benedict, 1978]

Band	Upper	Lower	Isotope	Center	Intensity
1	01101	00001	626	667.379	193.352
2	10002	01101	626	618.033	3.463
3	10001	01101	626	720.808	4.562
4	02201	01101	626	667.750	15.890
5	11102	10002	626	647.058	.563
6	11101	10002	626	791.452	.029
7	11102	02201	626	597.341	.130
8	11101	02201	626	741.736	.204
9	03301	02201	626	668.109	.979
10	11102	10001	626	544.203	.0068
11	12202	03301	626	581.794	.0050
12	12201	03301	626	757.497	.0088
13	12201	11102	626	828.265	.00054
14	20002	11102	626	738.643	.0081
15	11101	10001	626	688.678	.383
16	20002	11101	626	594.248	.0024
17	12202	11102	626	652.536	.044
18	20001	11101	626	720.289	.013
19	20003	11102	626	615.903	.018
<i>Isotopic Bands</i>					
1	01101	00001	636	648.484	2.171
2	10002	01101	636	617.336	.039
3	10001	01101	636	721.583	.051
4	02201	01101	636	648.785	.178
1	01101	00001	628	662.368	.790
2	10002	01101	628	597.062	.014
4	02201	01101	628	662.782	.064
1	01101	00001	627	664.735	.143

Intensities are in units of cm⁻¹ (atm cm)_{300K}⁻¹. Intensities include the effects of stimulated emission.

TABLE 8. Intensities Given by Drayson for the C¹²O₂¹⁶ Bands Included in Table 7 and Ratio of AFGL Band Intensities to Drayson Intensities

Band	Drayson Intensity, [cm ⁻¹ (atm cm) _{300K} ⁻¹]	AFGL Intensity/ Drayson Intensity
1	194.0	0.997
2	4.27	0.811
3	5.0	0.912
4	15.0	1.059
5	0.7	0.804
6	0.022	1.323
7	0.14	0.930
8	0.144	1.414
9	0.85	1.152
10	0.01	0.674
11	0.005	1.004
12	0.006	1.475
13	0.0007	0.777
14	0.0035	2.311
15	0.3	1.276
16	0.0036	0.661
17	0.045	0.973
18	0.005	2.580
19	0.015	1.200

Bands are listed in Table 7.

with observed integrated absorptions, it would be clearly desirable to use a smoother cutoff procedure.

On the basis of preliminary estimates, we do not expect that the results of more precise calculations of this type will change the absorptions by more than 1 or 2%.

b. Extension to Other Bands and Atmospheric Models

At present CO₂ levels, the only significant IR bands lie in the 12 to 18 μm region. This ceases to be the case when the mixing ratio is 10 times the present value. At mixing ratios of 3%, the 10-μm complex plays an important role in terrestrial thermal balance (S. B. Fels and M. D. Schwarzkopf, unpublished, 1979). We have found that the methods developed in this paper work equally well (with minor modifications) for the 10-μm bands. Tables of transmission functions for both the 15- and 10-μm complexes have been precalculated for a mixing ratio of 3.3% (by volume) and may be obtained from the authors.

c. Summary

In spite of the shortcomings discussed above, we believe that the computational simplicity and high potential accuracy of our algorithms make their use attractive, both as benchmarks and for routine use in GCM's. It is our intention to update the tables periodically, as required by new experimental developments and their use by other workers in this area.

6. TABLES OF TRANSMISSION FUNCTIONS

The tables of CO₂ transmission functions whose use has been discussed in section 3 are available on microfiche.¹ To conserve space, we print out only the lower atmosphere transmission functions for a standard temperature profile and 330 ppmv.

¹ The entire set of tables, along with this article, are available on microfiche where they are referred to as Tables 6-1 through 6-12. Order from American Geophysical Union, 2000 Florida Avenue, N.W., Washington, D.C. 20009. Document number J81002; \$1.00. Payment must accompany order.

TABLE 9. Fractional Difference (%) Using AFGL Absorption Data Compared With Drayson Data for a Mid-Latitude Sounding

TABLE 10. Comparison of Line Intensities for Selected Q-Branch Lines of Fundamental CO₂ Band Between *Planet et al.* [1979] and AFGL (Intensities are in Units cm⁻¹ (atm cm)_{300K}⁻¹)

<i>J</i>	Intensity	
	Planet	AFGL
4	2.99	3.12
6	4.15	4.35
8	5.18	5.36
10	5.82	6.16
12	6.73	6.74
14	6.78	7.07
16	6.69	7.15

TABLE 11. Comparison of Equivalent Widths (in cm⁻¹) of Plass From *p* = 0 to Selected Atmospheric Levels With Those of the Present Work, Obtained by Angular Integration of Absorptions

Height, km	50	30	25	15
Present	2.320	16.964	30.257	78.336
Plass	1.165	17.262	31.066	80.278

TABLE 12. Comparison of Cooling Rates of Present Work with Those Obtained by R. E. Dickinson (Private Communication, 1977) (in Deg/Day)

CO ₂ Bands	Height, km					
	49.5		53.0		56.0	
	Present Work	Dickinson	Present Work	Dickinson	Present Work	Dickinson
Fundamental, C ¹² O ₂ ¹⁶	3.10	3.24	2.93	2.95	2.29	2.21
Fundamental, total	4.17	4.29	4.01	4.16	3.45	3.36
First hot bands total	2.27	2.37	2.46	2.56	2.42	2.29
Second hot bands total	0.92	1.18	1.02	1.29	0.95	0.97
Total cooling rate	7.36	7.84	7.49	8.01	6.82	6.62

Dickinson's line widths, band intensities, and CO₂ mixing ratio are adjusted to be the same as in the present work. Because the standard atmosphere temperature profile has been used, there are no temperature corrections to be applied to our τ 's.

Acknowledgment. We are extremely grateful to R. Drayson, who provided us with the line-by-line transmission function program from which our own program evolved and who cheerfully answered numerous questions during the early phase of this work. The comparison with the results of R. Dickinson would not have been possible without the painstaking assistance of R. Dickinson over a period of several years. We wish to thank R. McClatchey for useful discussions of CO₂ line parameters. J. Kennedy typed and retyped a difficult manuscript with patience and skill.

REFERENCES

- Blake, D., and R. S. Lindzen, Effect of photochemical models on calculated equilibria and cooling rates in the stratosphere, *Mon. Weather Rev.*, **101**, 783–802, 1973.
- Burch, D. E., D. A. Gryvnak, R. R. Patty, and C. E. Bartky, Absorption of infrared radiant energy by CO₂ and H₂O, 4, Shapes of collision-broadened CO₂ lines, *J. Opt. Soc. Am.*, **59**, 267–280, 1969.
- Chou, M. D., and A. Arking, An infrared radiation routine for use in numerical atmospheric models, paper presented at the Third Conference on Atmospheric Radiation, Am. Meteorol. Soc., Boston, 1978.
- Curtis, A. R., A discussion on 'radiative balance': The computation of radiative heating rates in the atmosphere, *Proc. R. Soc. London Ser. A*, **236**, 156–159, 1956.
- Dickinson, R. E., Infrared radiative heating and cooling in the Venusian mesosphere, I, Global mean radiative equilibrium, *J. Atmos. Sci.*, **29**, 1531–1556, 1972.
- Dickinson, R. E., Methods of parameterization for infrared cooling between altitudes of 30 and 70 kilometers, *J. Geophys. Res.*, **78**, 4451–4457, 1973.
- Drayson, S. R., Atmospheric transmission in the CO₂ bands between 12 μ and 18 μ , *Appl. Opt.*, **5**, 385–391, 1967.
- Drayson, S. R., A listing of wavenumbers and intensities of carbon dioxide absorption lines between 12 and 20 μ m, *Rep. 036350-4-T*, Univ. of Mich., Ann Arbor, 1973.
- Ellingson, R. G., and J. C. Gille, An infrared radiative transfer model, I, Model description and comparison of observations with calculations, *J. Atmos. Sci.*, **35**, 523–545, 1978.
- Fels, S. B., Simple strategies for inclusion of Voigt effects in infrared cooling calculations, *Appl. Opt.*, **18**, 2634–2637, 1979.
- Fels, S. B., and L. D. Kaplan, A test of the role of longwave radiative transfer in a general circulation model, *J. Atmos. Sci.*, **33**, 779–789, 1975.
- Fels, S. B., J. D. Mahlman, M. D. Schwarzkopf, and R. W. Sinclair, Stratospheric sensitivity to perturbations in ozone and carbon dioxide: radiative and dynamical response, submitted to *J. Atmos. Sci.*, **37**, 2265–2297, 1980.
- Goody, R. M., and M. J. S. Belton, Radiative relaxation times for Mars, *Planet. Space Sci.*, **15**, 247–256, 1967.
- Gryvnak, D. A., and D. G. Burch, Infrared absorption by CO₂ and H₂O, *Rep. AFGL-TR-78-0154*, Air Force Geophys. Lab., Hanscom AFB, Bedford, Mass., 1978.
- Gryvnak, D. A., D. E. Burch, P. L. Alt, and D. K. Zgonc, Infrared absorption by CH₄, H₂O and CO₂, *Rep. AFGL-TR-76-0246*, Air Force Geophys. Lab., Hanscom AFB, Bedford, Mass. 1976.
- Howard, J. N., D. E. Burch, and D. Williams, Infrared transmission of synthetic atmospheres, 2, Absorption by carbon dioxide, *J. Opt. Soc. Am.*, **46**, 237–241, 1956.
- Hui, A. K., B. H. Armstrong, and A. A. Wray, Rapid computation of the Voigt and complex error functions, *Tech. Rep. G20-3357*, Palo Alto Sci. Center, IBM Corporation, Palo Alto, Calif., 1977.
- Manabe, S., and R. F. Strickler, On the thermal equilibrium of the atmosphere with convective adjustment, *J. Atmos. Sci.*, **21**, 361–385, 1964.
- McClatchey, R. A., W. S. Benedict, S. A. Clough, D. E. Burch, R. F. Calfee, K. Fox, C. S. Rothman, and J. S. Garing, AFCRL atmospheric absorption line parameters compilation, *Environ. Res. Pap. 434*, Air Force Cambridge Res. Lab., Hanscom AFB, Bedford, Mass., 1973.
- Murgatroyd, R. J., and R. M. Goody, Sources and sinks of radiative energy from 30 to 90 km, *Quart. J. R. Meteorol. Soc.*, **84**, 225–234, 1958.
- Planet, W. G., G. L. Tettener, and J. S. Knoll, Temperature dependence of intensities and widths of N₂-broadened lines in the 15 μ m CO₂ band from tunable laser measurements, *J. Quant. Spectrosc. Rad. Trans.*, **20**, 547–556, 1978.
- Planet, W. G., and G. L. Tettener, Temperature-dependent in-

- tensities and widths of N₂-broadened CO₂ lines at 15 μm for tunable laser measurements, *J. Quant. Spectrosc. Rad. Trans.*, 22, 345–354, 1979.
- Plass, G. N., The influence of the 15 micron carbon dioxide band on the atmospheric infrared cooling rate, *Quart. J. Roy. Meteorol. Soc.*, 82, 30–44, 1956.
- Plass, G. N., Infrared transmission studies, *Final Rep., SSD-TDR-62-127*, Space Systems Div., Air Force Systems Command, Los Angeles, Calif., 1963.
- Plass, G. N., The infrared absorption of carbon dioxide, *Appl. Opt.*, 3, 243–251, 1964.
- Ramanathan, V., Radiative transfer within the earth's troposphere and stratosphere: A simplified radiative-convective model, *J. Atmos. Sci.*, 33, 1330–1346, 1976.
- Rodgers, C. D., and C. D. Walshaw, The computation of infrared cooling rate in planetary atmospheres, *Quart. J. R. Meteorol. Soc.*, 92, 67–92, 1966.
- Rothman, L. S., and W. S. Benedict, Infrared energy levels and intensities of carbon dioxide, *Appl. Opt.*, 17, 2605–2611, 1978.
- Sasamori, T., The radiative cooling calculation for application to general circulation experiments, *J. Appl. Meteorol.*, 7, 721–729, 1968.
- Susskind, J., and T. Mo, Atmospheric absorption spectra near 2200 cm⁻¹ and 2400 cm⁻¹, paper presented at the Third Conference on Atmospheric Radiation, Am. Meteorol. Soc., Boston, 1978.
- Tettemer, G. L., and W. G. Planet, Intensities and pressure-broadened widths of CO₂ R-branch lines of 15 μm from tunable laser measurements, *J. Quant. Spectrosc. Rad. Trans.*, 23, 343–345, 1980.
- U.S. Air Force, *Handbook of Geophysics*, Macmillan, New York, 1960.
- Winters, B. H., S. Silverman, and W. S. Benedict, Line shape in the wing beyond the band head of the 4.3 μm band of CO₂, *J. Quant. Spectrosc. Rad. Trans.*, 4, 527–537, 1964.

(Received January 17, 1980;
revised September 11, 1980;
accepted September 16, 1980.)